nature structural & molecular biology

The hidden energetics of ligand binding and activation in a glutamate receptor

Albert Y Lau[1,2] & Benoît Roux[1]

Ionotropic glutamate receptors (iGluRs) are ligand-gated ion channels that mediate most excitatory synaptic transmission in the central nervous system. The free energy of neurotransmitter binding to the ligand-binding domains (LBDs) of iGluRs is converted into useful work to drive receptor activation. We have computed the principal thermodynamic contributions from ligand docking and ligand-induced closure of LBDs for nine ligands of GluA2 using all-atom molecular dynamics free energy simulations. We have validated the results by comparison with experimentally measured apparent affinities to the isolated LBD. Features in the free energy landscapes that govern closure of LBDs are key determinants of binding free energies. An analysis of accessible LBD conformations transposed into the context of an intact GluA2 receptor revealed that the relative displacement of specific diagonal subunits in the tetrameric structure may be key to the action of partial agonists.

Ionotropic glutamate receptors are tetrameric protein complexes that transduce chemical signals carried by neurotransmitter molecules into electrical impulses propagated in the postsynaptic neuron. Each protein subunit includes an N-terminal domain (ATD) and a cytoplasmic C-terminal domain (CTD), which are involved in receptor assembly, trafficking and regulation, a transmembrane domain (TMD) that forms the membrane-spanning ion channel, and a ligand-binding domain (LBD) that is key to channel gating[1]. The binding of agonist molecules to the LBDs drives the opening of the transmembrane pore, thereby allowing cations to flow across the cell membrane to trigger the generation of a nerve impulse. Full agonists such as glutamate have the highest levels of efficacy at the receptor, whereas antagonists block receptor activation and partial agonists produce submaximal responses when applied at saturating concentrations.

The LBD is a flexible, clamshell-shaped protein that makes a conformational transition from an open to a closed state when it binds an agonist molecule in the cleft that separates its two lobes. Four LBDs are tethered to the TMD by short linkers, and when the LBDs close down to encapsulate the ligand, the local conformational change is assumed to force the opening of the transmembrane channel[2]. It is important to understand how the binding of different ligands leads to or inhibits the activation of the receptor. One possible mechanism, inferred from crystal structures of LBD–ligand complexes, is that ligand efficacy is directly correlated with the amount of cleft closure induced by the bound ligand[3]. There are discrepancies, however, which are not fully understood. For example, the LBDs of the GluN1 and GluK1 subunits have been shown to close fully even when bound to partial agonists[4,5]. The relative twist between the two lobes has also been suggested to be important[6–8]. Such observations suggest that a purely 'structural' explanation that is based solely on cleft closure is not completely satisfactory.

Alternatively, a 'dynamical' mechanistic perspective might be that full agonists succeed in tightly closing the clamshell through strong interactions between the LBD and the ligand, whereas bound partial agonists exert only weak cleft-closing forces and thus cannot prevent transient fluctuations that lead to partial reopening of the LBD. The measured binding affinities of some antagonists to the isolated GluA2 LBD are stronger than the affinities of some agonists, which suggest that only a fraction of the total binding free energy is available to close the LBD and activate the receptor[3,9]. The efficacy of an agonist can also be modulated by the stability of the closed LBD–agonist complex[10–13].

A contrast can be drawn between the structural and dynamical views, in which function is explained either by X-ray structures of the LBD in complex with different ligands or by the fluctuations and transient excursions of the LBD away from a static conformation, although both are necessarily oversimplified. Nevertheless, it is difficult to achieve a deeper understanding of the mechanism of activation of iGluR receptors without a detailed dissection of the different thermodynamic contributions associated with ligand binding and LBD closure, which provide the link between structure and dynamics. Although such thermodynamic information is central to understanding the activation mechanism of ligand-gated receptors, it is difficult to access directly by experimental means and remains essentially 'hidden' from direct observations. We have determined the free energy contributions that govern the distinct subprocesses of ligand docking and LBD closure for the *Rattus norvegicus* GluA2 receptor with nine different ligands using all-atom molecular dynamics simulations with explicit solvent molecules. We used the results to analyze LBD conformational distributions in the context of a full-length receptor and found key structural asymmetries that might influence activation.

[1]Department of Biochemistry and Molecular Biology, The University of Chicago, Chicago, Illinois, USA. [2]Present address: Department of Biophysics and Biophysical Chemistry, Johns Hopkins University School of Medicine, Baltimore, Maryland, USA.

Received 17 August 2010; accepted 30 November 2010; published online 13 February 2011; doi:10.1038/nsmb.2010

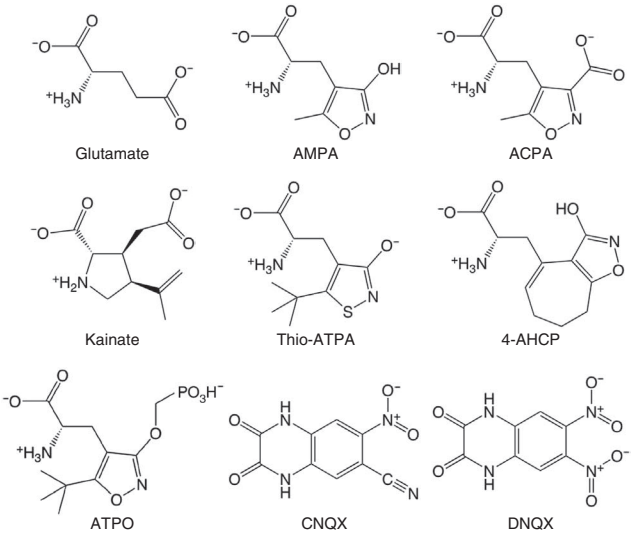

Figure 1 Ligands of GluA2. The full agonists (top) are glutamate, α-amino-3-hydroxy-5-methyl-4-isoxazole propionic acid (AMPA), and (*S*)-2-amino-3-(3-carboxy-5-methylisoxazol-4-yl)propionic acid (ACPA). The partial agonists (middle) are kainate, (*S*)-2-amino-3-(3-hydroxy-5-*tert*-butyl-4-isothiazolyl)propionic acid (thio-ATPA), and (*S*)-2-amino-3-(3-hydroxy-7,8-dihydro-6*H*-cyclohepta[*d*]-4-isoxazolyl)propionic acid (4-AHCP). The antagonists (bottom) are (*S*)-2-amino-3-[5-tert-butyl-3-(phosphonomethoxy)-4-isoxazolyl]propionic acid (ATPO), 6-cyano-7-nitroquinoxaline-2,3-dione (CNQX), and 6,7-dinitroquinoxaline-2,3 dione (DNQX). Crystal structures of each of these ligands in complex with the GluA2 LBD were used for our molecular models[3,6,9,22–24].

RESULTS

Ligand-binding free energy calculations

To provide a broad perspective on the different modes of ligand action on the GluA2 receptor, we characterized the binding of three full agonists, three partial agonists and three antagonists (**Fig. 1**) using all-atom molecular dynamics simulations with explicit solvent. We computed the absolute binding free energies between each ligand and the flexible LBD as the sum of separate contributions corresponding to different steps of the ligand-binding process (see Online Methods). This computational approach, which was based on umbrella sampling potential of mean force (PMF) calculations, follows from a rigorous statistical mechanical formulation of noncovalent binding[14] (see **Supplementary Methods**, Theory). This procedure, which involves applied restraints, limits the amount of configurational space the ligand must sample while rigorously accounting for the associated free energies (**Fig. 2** and **Supplementary Figs. 1** and **2**). The computations represent a total aggregate simulation time of ~1 μs.

Spectroscopic and stopped-flow kinetic analyses indicate that ligands dock into a pocket formed by residues Pro478, Thr480 and Arg485 in lobe 1 before forming additional interactions with residues in lobe 2 (refs. 9,15,16). In the ligand-docking simulations, the LBD was restrained to an open conformation that allows a ligand to access its docking site ((ξ_1, ξ_2) = (14.4 Å, 13.7 Å)). Atomic-scale fluctuations around the open conformation are sampled, but closure of the LBD is not permitted. This conformation is within the computed free energy basin of the apo LBD and is therefore predicted to be visited frequently by the protein before ligand docking (**Fig. 2** and **Supplementary Fig. 3**).

The free energy contributions from both ligand docking ($\Delta G^{(\circ)}_{dock}$) and LBD closure ($\Delta G_{close}$) are required to correctly calculate the binding affinity between a ligand and a flexible protein. The docking step, by itself, was insufficient to predict affinity, as evidenced by the lack of correlation between $\Delta G^{(\circ)}_{dock}$ and the experimentally measured binding free energies (**Fig. 3a**). This is expected because docking is only one of several contributions that must be taken into account (see equation (1) in Online Methods). There was a moderate correlation between ΔG_{close} and the experimental values (**Fig. 3b**), but a very strong correlation when we considered the sum of the docking and LBD closure components, $\Delta G^{(\circ)}_{bind} = \Delta G^{(\circ)}_{dock} + \Delta G_{close}$ (**Fig. 3c**). The correlation coefficient R^2 was 0.879, with a slope of 1.039, implying that the computed binding affinities agree well with experimental measurements. Glutamate and thio-ATPA (see **Fig. 1** for details of ligands) had positive values of ΔG_{dock}, indicating that docking into the LBD from bulk solvent is an unfavorable process for these two ligands (**Fig. 3a**). However, the substantial gain in free energy from LBD closure compensated for the unfavorable $\Delta G^{(\circ)}_{dock}$ and resulted in a favorable ΔG_{bind} (**Fig. 3b**,**c**). The antagonists CNQX

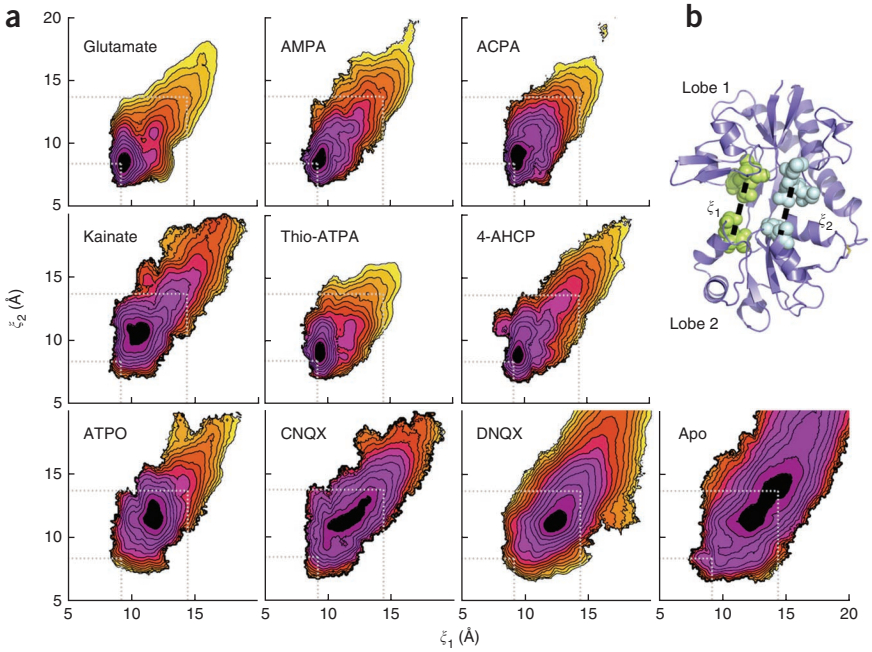

Figure 2 LBD conformational distributions. (**a**) The free energy landscapes that govern LBD closure for the holo and apo proteins calculated from all-atom umbrella sampling molecular dynamics simulations with explicit solvent. Each contour line corresponds to 1 kcal mol^{-1}, with the darker colors indicating more favorable conformations. The free energy minimum associated with the most closed conformation is for AMPA: (ξ_1, ξ_2) = (9.2 Å, 8.4 Å). The conformation used for the ligand-docking simulations is (14.4 Å, 13.7 Å). These locations are indicated by the dotted lines in each panel. (**b**) The two-dimensional order parameter (ξ_1, ξ_2) describing closure of the GluA2 LBD. Each distance (dashed line) is measured between the centers of mass of the residues whose atoms are shown as spheres. The crystal structure of the open, apo LBD (1FTO) is shown.

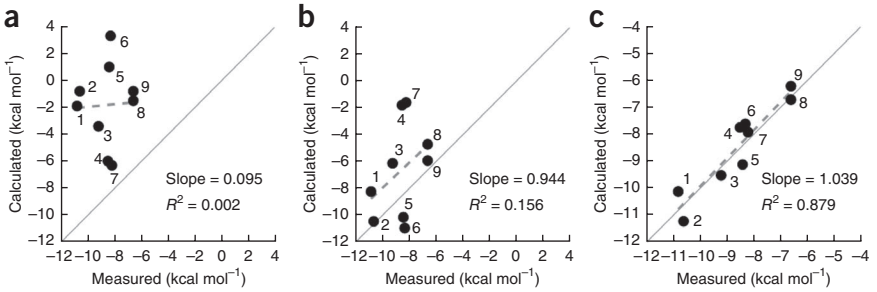

Figure 3 Comparison of calculated free energy contributions with experimentally measured effective ligand-binding affinities to the isolated GluA2 LBD. (**a**) Calculated $\Delta G^{(o)}_{dock}$. (**b**) Calculated ΔG_{close}. (**c**) Calculated $\Delta G^{(o)}_{bind} = \Delta G^{(o)}_{dock} + \Delta G_{close}$. In each plot, the solid line, which has a slope of 1, indicates perfect agreement between the calculated and experimental values. The dashed lines are linear regression fits to the data, and their slopes and correlation coefficients are shown. Each ligand is marked numerically in increasing order from the highest experimentally measured affinity to the lowest (**Supplementary Table 1**): 1, AMPA; 2, ACPA; 3, 4-AHCP; 4, CNQX; 5, glutamate; 6, thio-ATPA; 7, DNQX; 8, kainate; and 9, ATPO.

and DNQX had the most favorable docking free energies among the nine ligands. Values of ΔG_{close} were negative for all nine ligands, but CNQX and DNQX had the lowest ΔG_{close} values. See **Supplementary Table 1** for all components of the absolute binding free energies for all nine ligands. The free energy contributions for glutamate and kainate were consistent with hydrogen deuterium exchange measurements[17]. The fact that CNQX had a broader free energy basin than DNQX was also consistent with the hydrogen deuterium exchange measurements, reflecting lobe dynamics for CNQX that are not observed for DNQX.

A practical issue is whether the charged ligands tend to change their protonation states upon binding to the LBD. Free energy perturbation (FEP) calculations indicated that the ionizable groups on the ligands can be modeled to retain their bulk solvent protonation states, even when fully bound (**Fig. 1**, **Supplementary Table 2** and **Supplementary Methods**). These states agree with Fourier transform infrared measurements[18]. Calculation of the binding free energy for alternate protonation states of AMPA and 4-AHCP—states determined to be inappropriate—gave values that agreed less well with the experimental measurements (**Supplementary Table 3**).

Free energy landscapes are key for evaluating binding

Having validated the computational methodology and the molecular dynamics simulations by comparing the results of the calculations with experimentally measured dissociation constants for nine ligands, we investigated the role of the individual free energy contributions that are 'hidden' in the total binding free energy on receptor activation. In particular, we asked whether the amount of free energy associated with LBD closure ΔG_{close}—clearly a key component in receptor activation—is accurately reflected in crystal structures of the LBD–ligand complexes.

The calculated ΔG_{close} and the extent of LBD closure seen in the crystal structures relative to the AMPA-bound structure were only weakly correlated ($R^2 = 0.569$; **Supplementary Fig. 4**), suggesting that the extent of closure, by itself, cannot account for the free energy associated with the protein's conformational transition. Therefore, the LBD free energy landscapes (**Fig. 2**) seem to be crucial for assessing ΔG_{close}.

All the free energy landscapes featured a single major free energy basin. The locations of the global free energy minima for the nine ligands were in good agreement with the crystal structure conformations of each LBD–ligand complex. The largest discrepancy was observed for kainate, where the predicted 'most favored' LBD conformation was more open than observed crystallographically ($(\Delta\xi_1, \Delta\xi_2) = (1.2\ Å, 1.4\ Å)$), the crystal structure conformation being higher in free energy by ~1.8 kcal mol^{-1}. The kainate landscape suggested that this weak partial agonist may stabilize a relatively open LBD conformation, but rare transitions to more closed conformations could trigger channel activation. The locations of these minima for the nine ligands were generally segregated as expected when ranked in terms of the effective one-dimensional coordinate $(\xi_1 + \xi_2)/2$: full agonists < partial agonists < antagonists (**Fig. 2** and **Supplementary Table 4**).

The detailed topological features in the different landscapes, as well as the number and shapes of shallow metastable states that surrounded the basins, differed among the nine ligands, even within the full agonist, partial agonist and antagonist classes. A metastable state

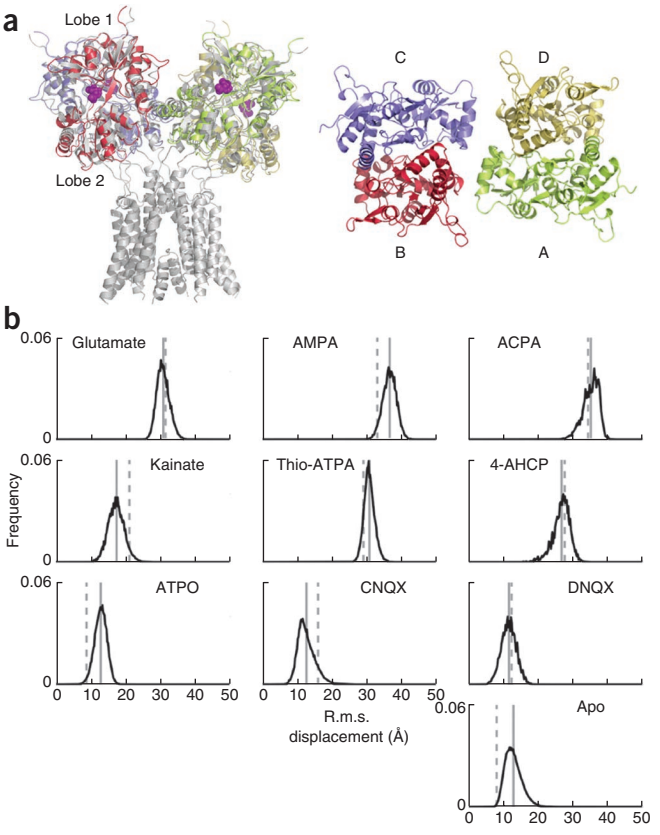

Figure 4 LBD conformational distributions in the context of an intact receptor. (**a**) Left, superposition of LBD conformations spanning the free energy landscapes onto the crystal structure of the intact GluA2 receptor (gray[2]; the ATD is not shown). The LBDs were superimposed only in lobe 1. Right, labeling of the four LBDs in an intact iGluR, as viewed from above. The LBDs assemble as a pair of dimers, where A–D is one dimer and B–C is the other. (**b**) R.m.s. displacement distributions of LBD conformations relative to the intact receptor. The r.m.s. displacement was measured in regions in lobe 2 (see Online Methods). The solid line indicates the average r.m.s. displacement (**Supplementary Table 5**). The dashed line indicates the r.m.s. displacement measured from the isolated LBD–ligand crystal structure.

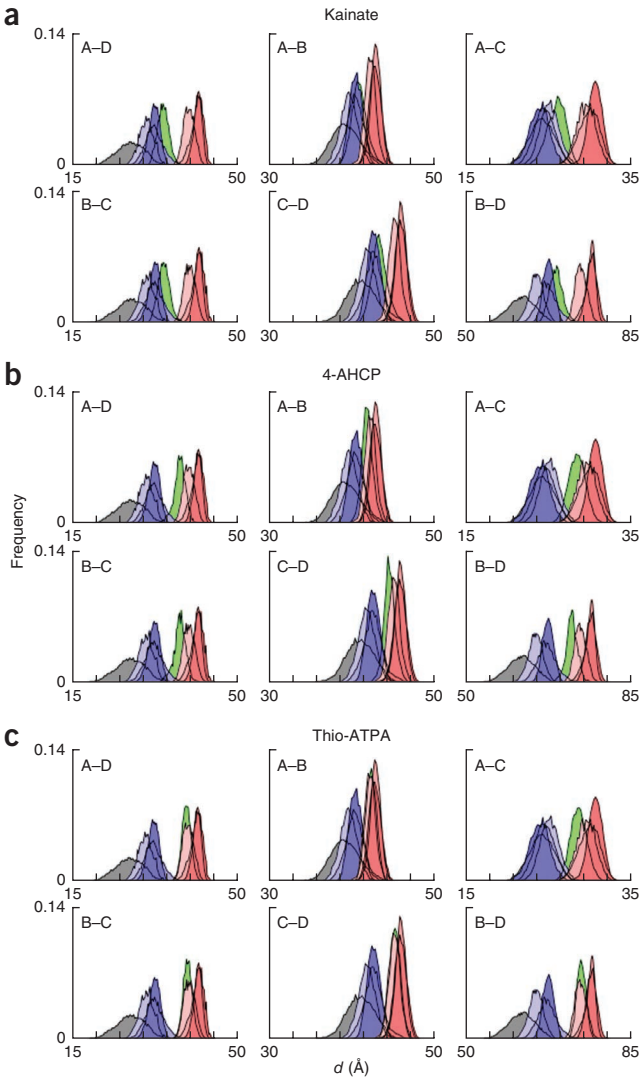

Figure 5 Inter-LBD distance distributions. LBD conformations were superimposed onto the intact GluA2 structure (**Fig. 4**), and the pairwise distances were measured between regions in lobe 2 (see Online Methods). The apo LBD is gray, the LBD–antagonist complexes are blue and the LBD–full agonist complexes are red. The LBD–partial agonist complexes for kainate (**a**), 4-AHCP (**b**) and thio-ATPA (**c**) are green. See **Supplementary Table 5** for statistics and the distances measured using the isolated LBD–ligand crystal structures.

in the glutamate landscape that corresponds to the largest cleft opening at which the ligand forms interactions with both lobes 1 and 2 has been described[19]. This conformation is $(\xi_1, \xi_2) \approx (12.0\ \text{Å}, 11.0\ \text{Å})$. We found topological features resembling finger-like extensions from the free energy basin in a similar location in the AMPA, thio-ATPA and 4-AHCP landscapes (**Fig. 2** and **Supplementary Fig. 5**). The topologies of the glutamate and thio-ATPA landscapes suggest that LBD closure from $(\xi_1, \xi_2) = (12.0\ \text{Å}, 11.0\ \text{Å})$ proceed first along ξ_2 and then along ξ_1. Conversely, the AMPA landscape suggests closure first along ξ_1 followed by ξ_2. Either trajectory seems plausible for 4-AHCP. The broad, shallow basin for ACPA suggests a more diffuse pathway of closure. For kainate and the antagonists, $(\xi_1, \xi_2) = (12.0\ \text{Å}, 11.0\ \text{Å})$ is near the free energy minimum. Free energy landscapes for two LBD mutants, T686A and T686S, have been described[19] and were consistent with experimental evidence that Thr686 mutations destabilize cleft closure[10].

LBD conformational distributions in an intact receptor

It is of interest to investigate how the local conformational change in the LBD might affect the TMD in the context of an intact full-length receptor using the present set of molecular dynamics free energy landscapes. To address this question, we transposed LBD snapshots spanning the free energy landscapes taken from the molecular dynamics simulations onto the crystal structure of an intact GluA2 receptor[2] (**Fig. 4a**). We superimposed only the residues in lobe 1 of the LBD, thereby preserving the back-to-back dimer interfaces as well as the relative dispositions of all four LBDs with respect to the ATDs. We assembled all tetrameric combinations of snapshot configurations. We obtained the proper Boltzmann weight of each snapshot, $p(\xi_1, \xi_2)$, directly from the free energy landscapes, $p(\xi_1,\xi_2) \propto \exp\left[-\beta W(\xi_1,\xi_2)\right]$, where $\beta^{-1} = k_B T$ is the Boltzmann constant multiplied by temperature. This structural analysis therefore reflects an equilibrium ensemble of the complexes in the different accessible states, and also assumes that each LBD opens and closes independently of the others. We then calculated the following Boltzmann-weighted displacements: the root-mean-squared (r.m.s.) displacement between the superimposed LBD tetramer and the LBD tetramer from the crystallized GluA2 receptor; and the six pairwise distances between the LBDs. The r.m.s. displacements and distances involve a selection of residues in lobe 2 near the region that connects to the TMD (see Online Methods). We measured the r.m.s. displacement with respect to the Cα atoms, and the pairwise distances between the centers of mass of these atoms.

The LBDs of the intact GluA2 structure are in open conformations as they are bound to the antagonist ZK200775 (ref. 20). LBD–agonist conformations deviated more than the LBD–antagonist or apo LBD conformations. Histograms of the Boltzmann-weighted r.m.s. displacement measurements in the LBDs for the holo and apo forms are shown in **Figure 4b**. Overall, the averages of the r.m.s. displacement distributions came up as expected, with full agonists > partial agonists > antagonists (**Supplementary Table 5**). For some ligands, such as glutamate, the average r.m.s. displacement closely agreed with that obtained by directly superimposing the LBD–ligand crystal structure. For other ligands, such as AMPA, and for the apo LBD, there were pronounced differences between the thermal averages and the crystal structures. These differences suggest that the crystal structure conformations of the different LBD–ligand complexes do not always quantitatively account for the amount of conformational change that ligand binding can transmit to the TMD. For example, the LBD–AMPA crystal structure underestimated the average amount of conformational change the LBD samples upon binding AMPA, and the LBD–kainate crystal structure overestimated it. As the (ξ_1, ξ_2) corresponding to the computed global free energy minima agreed well with the (ξ_1, ξ_2) of the respective crystal structures (**Supplementary Table 4**), the differences in the r.m.s. displacement distributions arises necessarily from the features in the free energy landscapes that govern LBD closure.

A different perspective on the amount of useful work that the LBDs can transmit to the TMD is revealed by considering the Boltzmann-weighted pairwise distances between lobes 2 for the holo and apo LBDs. Histograms of these measurements (**Fig. 5**) provide mechanistic inferences in terms of the amount of conformational change that can be transmitted to the ion-channel gate by ligand-bound LBDs in the context of a full-length receptor. The antagonist and apo distributions were clearly distinct from the full agonist distributions, although there was some overlap in the tails. The width of the distribution is related to how strongly the ligand stabilizes the LBD conformation around

its free energy minimum (see **Supplementary Table 5** for statistics on the distributions). These widths varied among the ligands, but there was no strong correlation with ligand type. The average values of the distributions for kainate were closer to the averages for the antagonists than to those for the full agonists. This observation is consistent with kainate being a weak partial agonist. By contrast, the averages of the distributions for 4-AHCP were closer to the averages for the full agonists than to those for the antagonists. The 4-AHCP peaks were shifted to the left relative to the full agonists, indicating a reduced capacity to open the ion channel. Surprisingly, the thio-ATPA distributions almost completely coincided with the distributions for glutamate in all but the A-C distance. For the diagonal A-C pair, thio-ATPA was shifted to the left of the full agonists. The reduced displacement solely in the A–C direction relative to glutamate may explain why thio-ATPA acts as a strong partial agonist rather than as a full agonist. When the crystal structures of LBD–glutamate and LBD–(thio-ATPA) were superimposed onto the intact GluA2 structure, most inter–lobe 2 distances were smaller for the thio-ATPA complex than for the glutamate complex (**Supplementary Table 5**). However, the present analysis of equilibrium conformational distributions suggests that this tempered agonism stems only from reduced displacement along the diagonal A–C direction rather than from several directions. Subunit nonequivalence has also been suggested for GluK2 receptors[21]. Another noteworthy observation is that the B–D distributions (the other diagonal direction) resembled the A–D and B–C distributions with an offset distance of about 35 Å. This similarity suggests that a given ligand induces an equivalent amount of displacement in these three directions.

DISCUSSION

The analysis presented here provides a first dissection of the energetic components that govern the molecular conformations and interactions that are likely to be crucial for the function of iGluRs. Topological features in the free energy landscapes that govern closure of LBDs seem to be important for evaluating the efficacy of agonists. Although the results deduced by transposing the calculated free energy landscapes of isolated LBDs onto the full-length GluA2 receptor are partly speculative, they provide a useful roadmap for the design of experiments and interpretation of results. These receptors are allosteric proteins in which the effects triggered by ligand binding are propagated over an appreciable distance through the molecule. We have established a quantitative account of the (hidden) relationship between structure and dynamics for the LBDs using molecular dynamics free energy simulations. The conformational dynamics of LBD assemblies in complex with different ligands, deduced from the free energy landscapes, build upon the information provided by crystal structures of LBD–ligand complexes, thereby offering a more complete understanding of how the actions of full agonists, partial agonists and antagonists are associated with LBD closure. The present computational framework could be extended to the analysis of other ligand-gated receptors and their activation characteristics.

METHODS

Methods and any associated references are available in the online version of the paper at http://www.nature.com/nsmb/.

Note: Supplementary information is available on the Nature Structural & Molecular Biology website.

ACKNOWLEDGMENTS

We thank E. Gouaux, V. Jayaraman, C. Landes, M. Mayer, R. Oswald and H. Weinstein for review of the manuscript, and W. Gan for discussions. This work was supported by grant MCB-0920261 from the National Science Foundation and grant GM062342 from the US National Institutes of Health. Computational resources were provided by the National Center for Supercomputing Applications (NCSA) through grant MCA01S018.

AUTHOR CONTRIBUTIONS

A.Y.L. and B.R. designed the research, analyzed the data and wrote the manuscript. A.Y.L. performed the computations.

COMPETING FINANCIAL INTERESTS

The authors declare no competing financial interests.

Published online at http://www.nature.com/nsmb/.
Reprints and permissions information is available online at http://npg.nature.com/reprintsandpermissions/.

1. Mayer, M.L. Glutamate receptors at atomic resolution. *Nature* **440**, 456–462 (2006).
2. Sobolevsky, A.I., Rosconi, M.P. & Gouaux, E. X-ray structure, symmetry and mechanism of an AMPA-subtype glutamate receptor. *Nature* **462**, 745–756 (2009).
3. Armstrong, N. & Gouaux, E. Mechanisms for activation and antagonism of an AMPA-sensitive glutamate receptor: crystal structures of the GluR2 ligand binding core. *Neuron* **28**, 165–181 (2000).
4. Inanobe, A., Furukawa, H. & Gouaux, E. Mechanism of partial agonist action at the NR1 subunit of NMDA receptors. *Neuron* **47**, 71–84 (2005).
5. Frydenvang, K. *et al.* Full domain closure of the ligand-binding core of the ionotropic glutamate receptor iGluR5 induced by the high affinity agonist dysiherbaine and the functional antagonist 8,9-dideoxyneodysiherbaine. *J. Biol. Chem.* **284**, 14219–14229 (2009).
6. Holm, M.M., Lunn, M.L., Traynelis, S.F., Kastrup, J.S. & Egebjerg, J. Structural determinants of agonist-specific kinetics at the ionotropic glutamate receptor 2. *Proc. Natl. Acad. Sci. USA* **102**, 12053–12058 (2005).
7. Bjerrum, E.J. & Biggin, P.C. Rigid body essential X-ray crystallography: distinguishing the bend and twist of glutamate receptor ligand binding domains. *Proteins* **72**, 434–446 (2008).
8. Birdsey-Benson, A., Gill, A., Henderson, L.P. & Madden, D.R. Enhanced efficacy without further cleft closure: reevaluating twist as a source of agonist efficacy in AMPA receptors. *J. Neurosci.* **30**, 1463–1470 (2010).
9. Ahmed, A.H. *et al.* Mechanisms of antagonism of the GluR2 AMPA receptor: structure and dynamics of the complex of two willardiine antagonists with the glutamate binding domain. *Biochemistry* **48**, 3894–3903 (2009).
10. Robert, A., Armstrong, N., Gouaux, J.E. & Howe, J.R. AMPA receptor binding cleft mutations that alter affinity, efficacy, and recovery from desensitization. *J. Neurosci.* **25**, 3752–3762 (2005).
11. Weston, M.C., Gertler, C., Mayer, M.L. & Rosenmund, C. Interdomain interactions in AMPA and kainate receptors regulate affinity for glutamate. *J. Neurosci.* **26**, 7650–7658 (2006).
12. Zhang, W., Cho, Y., Lolis, E. & Howe, J.R. Structural and single-channel results indicate that the rates of ligand binding domain closing and opening directly impact AMPA receptor gating. *J. Neurosci.* **28**, 932–943 (2008).
13. Maltsev, A.S., Ahmed, A.H., Fenwick, M.K., Jane, D.E. & Oswald, R.E. Mechanism of partial agonism at the GluR2 AMPA receptor: measurements of lobe orientation in solution. *Biochemistry* **47**, 10600–10610 (2008).
14. Woo, H.J. & Roux, B. Calculation of absolute protein-ligand binding free energy from computer simulations. *Proc. Natl. Acad. Sci. USA* **102**, 6825–6830 (2005).
15. Abele, R., Keinänen, K. & Madden, D.R. Agonist-induced isomerization in a glutamate receptor ligand-binding domain. *J. Biol. Chem.* **275**, 21355–21363 (2000).
16. Cheng, Q., Du, M., Ramanoudjame, G. & Jayaraman, V. Evolution of glutamate interactions during binding to a glutamate receptor. *Nat. Chem. Biol.* **1**, 329–332 (2005).
17. Fenwick, M.K. & Oswald, R.E. On the mechanisms of alpha-amino-3-hydroxy-5-methylisoxazole-4-propionic acid (AMPA) receptor binding to glutamate and kainate. *J. Biol. Chem.* **285**, 12334–12343 (2010).
18. Cheng, Q. & Jayaraman, V. Chemistry and conformation of the ligand-binding domain of GluR2 subtype of glutamate receptors. *J. Biol. Chem.* **279**, 26346–26350 (2004).
19. Lau, A.Y. & Roux, B. The free energy landscapes governing conformational changes in a glutamate receptor ligand-binding domain. *Structure* **15**, 1203–1214 (2007).
20. Turski, L. *et al.* ZK200775: a phosphonate quinoxalinedione AMPA antagonist for neuroprotection in stroke and trauma. *Proc. Natl. Acad. Sci. USA* **95**, 10960–10965 (1998).
21. Das, U., Kumar, J., Mayer, M.L. & Plested, A.J.R. Domain organization and function in GluK2 subtype kainate receptors. *Proc. Natl. Acad. Sci. USA* **107**, 8463–8468 (2010).
22. Hogner, A. *et al.* Structural basis for AMPA receptor activation and ligand selectivity: crystal structures of five agonist complexes with the GluR2 ligand-binding core. *J. Mol. Biol.* **322**, 93–109 (2002).
23. Nielsen, B.B. *et al.* Exploring the GluR2 ligand-binding core in complex with the bicyclical AMPA analogue (*S*)-4-AHCP. *FEBS J.* **272**, 1639–1648 (2005).
24. Hogner, A. *et al.* Competitive antagonism of AMPA receptors by ligands of different classes: crystal structure of ATPO bound to the GluR2 ligand-binding core, in comparison with DNQX. *J. Med. Chem.* **46**, 214–221 (2003).

ONLINE METHODS

Ligand-binding free energies. The absolute free energy associated with binding a ligand to a flexible protein receptor is written as

$$\Delta G_{\text{bind}}^{(\circ)} = \Delta G_{\text{p, bulk}} + \Delta G_{\text{c, bulk}} + \Delta G_{\text{o, bulk}} - \Delta G_{\text{a, site}} - \Delta G_{\text{o, site}} - \Delta G_{\text{c, site}} - \Delta G_{\text{p, site}} - k_{\text{B}}T \ln\left(C^{\circ} S^{*} I^{*}\right), \quad (1)$$

where the superscript $(\circ)$ indicates the standard reference state, and $k_{\text{B}}T$ is the Boltzmann constant multiplied by temperature. The protein's conformational potential of mean force (PMF), or free energy landscape, has a key role in the formulation leading to equation (1). $\Delta G_{\text{p, bulk}}$ and $\Delta G_{\text{p, site}}$ are the free energies associated with restraining the protein in an open conformation when the ligand is either in the bulk solvent region (apo protein) or in its docking site (**Fig. 2**, **Supplementary Fig. 3** and **Supplementary Methods**, Theory). $\Delta G_{\text{c, bulk}}$, $\Delta G_{\text{o, bulk}}$, $\Delta G_{\text{a, site}}$, $\Delta G_{\text{o, site}}$ and $\Delta G_{\text{c, site}}$ are the free energies that correspond to the act of applying conformational, orientational and axial restraints on the ligand when it is in the bulk and then removing them after the ligand has been inserted into the docking site, respectively (**Supplementary Figs. 1** and **2**). The last term in equation (1) characterizes insertion of the ligand into the docking site and is defined in **Supplementary Methods**, Theory. The free energy of LBD closure is $\Delta G_{\text{close}} = \left[\Delta G_{\text{p, bulk}} - \Delta G_{\text{p, site}}\right]$. ΔG_{close} includes intra-LBD energetics as well as interactions between the LBD and the ligand.

For an inflexible receptor, $\Delta G_{\text{p, bulk}} = \Delta G_{\text{p, site}} = 0$, and the absolute free energy for protein-ligand docking can be expressed as[14]

$$\Delta G_{\text{dock}}^{(\circ)} = \Delta G_{\text{c, bulk}} + \Delta G_{\text{o, bulk}} - \Delta G_{\text{a, site}} - \Delta G_{\text{o, site}} - \Delta G_{\text{c, site}} - k_{\text{B}}T \ln\left(C^{\circ} S^{*} I^{*}\right) \quad (2)$$

Atomic models. The atomic models for the GluA2 S1S2 LBD monomer–ligand complexes were constructed from the following Protein Data Bank (PDB) X-ray crystal structures: 1FTJ (glutamate), 1FTM (AMPA), 1M5E (ACPA), 1FTK (kainate), 2AIX (thio-ATPA), 1WVJ (4-AHCP), 1N0T (ATPO), 3B7D (CNQX), 1FTL (DNQX) and 1FTO (apo)[3,6,9,22–24]. Chain A for each entry was used. This choice was arbitrary, but given the relatively small conformational differences among the different chains in each asymmetric unit and the presence of thermal fluctuations in the simulations, the results are not expected to be sensitive to small differences in the starting conditions. The model for the intact GluA2 receptor was constructed from 3KG2 (ref. 2). Missing amino acids were built using the MODLOOP server[25], and missing side chains were built using the program SCWRL[26]. Crystallographic waters in the ligand-binding cleft were included in our models. The software package Antechamber[27] was used to obtain generalized Amber force field (GAFF) parameters[28] for AMPA, ACPA, kainate, thio-ATPA, 4-AHCP, ATPO and CNQX, adapted for use with the CHARMM PARAM27 all-atom force field[29]. Geometry optimization of the molecules was performed at the Hartree-Fock 6-31G* level of theory using the Gaussian 03 program[30]. Restrained electrostatic potential (RESP) charges were used. The CHARMM PARAM27 model for glutamate was used, and DNQX was parameterized as described[19]. Molecular graphics images were generated using PyMOL (http://www.pymol.org/). Chemical structure images were generated using ChemDraw (http://www.cambridgesoft.com/).

Protein free energy landscapes, $W(\xi_1, \xi_2)$. A two-dimensional order parameter (ξ_1, ξ_2) is used to describe the large-scale conformational transitions of the LBD (**Fig. 2**). ξ_1 describes the distance between the centers of mass (COMs) of residues 479–481 in lobe 1 and residues 654–655 in lobe 2. ξ_2 describes the distance between the COM of residues 401–403 in lobe 1 and residues 686–687 in lobe 2. Starting coordinates for the umbrella sampling windows were obtained by using a targeted (biased-potential) molecular dynamics procedure to generate conformations positioned in 1-Å increments along ξ_1 and ξ_2, originating with the LBD–ligand crystal structure. In generating the starting conformations, we applied r.m.s. displacement restraints separately to each lobe of the LBD (lobe 1: residues 394–495 and 732–771; lobe 2: residues 500–728), and the ligands were restrained to remain bound to R485 in order to be consistent with the 'dock-lock' mechanism of iGluR ligand binding[15,16] in which the ligand is suggested to dock to lobe 1 before LBD closure. We used 96 windows for computing the AMPA, ACPA, kainate, thio-ATPA, 4-AHCP, ATPO and CNQX free energy landscapes, or potentials of mean force (PMFs). The total simulation time for each of these PMFs was ~40 ns. The number of atoms in each simulation system was ~36,000. The glutamate, DNQX and apo landscapes were computed as described[19]. We added Na^+ and Cl^- ions in the bulk solution to give 150 mM NaCl and an electrically neutral system. Periodic boundary conditions were used with an orthorhombic cell with approximate dimensions 88 Å × 72 Å × 60 Å. Harmonic biasing potentials with a force constant of 2.0 kcal mol^{-1} $Å^{-2}$ centered on the (ξ_1, ξ_2) positions were used. The COM biasing potentials were implemented with the MMFP module of CHARMM[31]. The distribution functions in (ξ_1, ξ_2) from all windows were unbiased and recombined using the weighted histogram analysis method (WHAM)[32,33] to calculate the PMF $W(\xi_1, \xi_2)$. The free energies $\Delta G_{\text{p, site}}$ and $\Delta G_{\text{p, bulk}}$ were obtained using equations (5a) and (5b) in **Supplementary Methods**, Theory. All simulations were performed using the program CHARMM[31] with explicit solvent.

Ligand translational PMF, $W(r)$. The PMF along the axis r, $W(r)$, was calculated using umbrella sampling simulations. r is the distance between the COM of residues Thr480+Tyr732 and the COM of the ligand. Each PMF was computed from 38 umbrella windows spaced 1 Å apart. A harmonic potential with a force constant of 1 kcal mol^{-1} $Å^{-2}$ was used. Equation (6) in **Supplementary Methods**, Theory was evaluated using $r^* = 40$ Å. The number of atoms in the system was ~46,000 (86 Å × 80 Å × 70 Å), and the total simulation time for each PMF was ~11 ns.

Tetrameric LBD assemblies. The computed LBD conformational ensemble was superimposed onto the crystal structure of the intact GluA2 at the Cα atoms of the following residue positions in lobe 1: 425–444, 464–494 and 734–755. This selection strives to preserve the LBD back-to-back dimer interface. The LBD r.m.s. displacement and inter-LBD distance measurements were performed at the Cα atoms of the following residue positions in lobe 2: 503–505 and 636–642. This selection flanks the region that connects the LBD to the TMD. For each free energy landscape $W(\xi_1, \xi_2)$, LBD conformations were selected spanning the entire landscape and superimposed onto the tetramer in all possible combinations, which totaled ~10^{13} different tetrameric assemblies.

25. Fiser, A. & Sali, A. ModLoop: automated modeling of loops in protein structures. *Bioinformatics* **19**, 2500–2501 (2003).
26. Krivov, G.G., Shapovalov, M.V. & Dunbrack, R.L. Jr. Improved prediction of protein side-chain conformations with SCWRL4. *Proteins* **77**, 778–795 (2009).
27. Wang, J., Wang, W., Kollman, P.A. & Case, D.A. Automatic atom type and bond type perception in molecular mechanical calculations. *J. Mol. Graph. Model.* **25**, 247–260 (2006).
28. Wang, J., Wolf, R.M., Caldwell, J.W., Kollman, P.A. & Case, D.A. Development and testing of a general AMBER force field. *J. Comput. Chem.* **25**, 1157–1174 (2004).
29. MacKerell, A.D. Jr. *et al.* All-atom empirical potential for molecular modeling and dynamics studies of proteins. *J. Phys. Chem. B* **102**, 3586–3616 (1998).
30. Frisch, M.J. *et al. Gaussian 03, Revision C.02.* (2004).
31. Brooks, B.R. *et al.* CHARMM: the biomolecular simulation program. *J. Comput. Chem.* **30**, 1545–1614 (2009).
32. Kumar, S., Rosenberg, J.M., Bouzida, D., Swendsen, R.H. & Kollman, P.A. The weighted histogram analysis method for free-energy calculations on biomolecules. I. The method. *J. Comput. Chem.* **13**, 1011–1021 (1992).
33. Souaille, M. & Roux, B. Extension to the weighted histogram analysis method: combining umbrella sampling with free energy calculations. *Comput. Phys. Commun.* **135**, 40–57 (2001).

doi:10.1038/nsmb.2010

based on an incomplete version of the $\alpha_6\beta_2$ ring seems more plausible (**Fig. 3**).

Finally, how has the pattern of activity regulation been conserved throughout evolution? The class III enzymes dimerize very differently and interact with a different type of β_2 subunit (**Fig. 1**). Moreover, the radical is generated on α_2 and can be used for many catalytic cycles before having to be regenerated[18], unlike class Ia enzymes, whose subunits have to reassociate on each cycle. Does the ATP cone affect subunit interactions or act on the α_2 subunit itself?

Given that $\alpha_4\beta_4$ oligomers of *E. coli* RNR, the first sign of higher-order association, were first observed by Brown and Reichard more than 40 years ago[19], it is exciting that the circle is now beginning to close on the structural basis for RNR activity regulation. The window that has just been opened is also a window of opportunity for future studies.

ACKNOWLEDGMENTS
The author thanks Anders Liljas for help with **Figure 2**.

COMPETING FINANCIAL INTERESTS
The author declares no competing financial interests.

1. Reichard, P. *Biochem. Biophys. Res. Commun.* **396**, 19–23 (2010).
2. Nordlund, P. & Reichard, P. *Annu. Rev. Biochem.* **75**, 681–706 (2006).
3. Fairman, J.W. *et al. Nat. Struct. Mol. Biol.* **18**, 316–322 (2011).
4. Eklund, H., Uhlin, U., Färnegårdh, M., Logan, D.T. & Nordlund, P. *Prog. Biophys. Mol. Biol.* **77**, 177–268 (2001).
5. Larsson, K.M., Logan, D.T. & Nordlund, P. *ACS Chem. Biol.* **5**, 933–942 (2010).
6. Uhlin, U. & Eklund, H. *Nature* **370**, 533–539 (1994).
7. Nordlund, P., Sjöberg, B.-M. & Eklund, H. *Nature* **345**, 593–598 (1990).
8. Uppsten, M., Färnegårdh, M., Domkin, V. & Uhlin, U. *J. Mol. Biol.* **359**, 365–377 (2006).
9. Eriksson, M. *et al. Structure* **5**, 1077–1092 (1997).
10. Larsson, K.-M., Andersson, J., Sjöberg, B.-M., Nordlund, P. & Logan, D.T. *Structure* **9**, 739–750 (2001).
11. Larsson, K.M. *et al. Nat. Struct. Mol. Biol.* **11**, 1142–1149 (2004).
12. Xu, H. *et al. Proc. Natl. Acad. Sci. USA* **103**, 4022–4027 (2006).
13. Kashlan, O.B., Scott, C.P., Lear, J.D. & Cooperman, B.S. *Biochemistry* **41**, 462–474 (2002).
14. Cooperman, B.S. & Kashlan, O.B. *Adv. Enzyme Regul.* **43**, 167–182 (2003).
15. Wang, J., Lohman, G.J. & Stubbe, J. *Proc. Natl. Acad. Sci. USA* **104**, 14324–14329 (2007).
16. Rofougaran, R., Vodnala, M. & Hofer, A. *J. Biol. Chem.* **281**, 27705–27711 (2006).
17. Rofougaran, R., Crona, M., Vodnala, M., Sjöberg, B.-M. & Hofer, A. *J. Biol. Chem.* **283**, 35310–35318 (2008).
18. Torrents, E., Eliasson, R., Wolpher, H., Gräslund, A. & Reichard, P. *J. Biol. Chem.* **276**, 33488–33494 (2001).
19. Brown, N.C. & Reichard, P. *J. Mol. Biol.* **46**, 39–55 (1969).
20. Logan, D.T., Andersson, J., Sjöberg, B.-M. & Nordlund, P. *Science* **283**, 1499–1504 (1999).
21. Sintchak, M.D., Arjara, G., Kellogg, B.A., Stubbe, J. & Drennan, C.L. *Nat. Struct. Biol.* **9**, 293–300 (2002).
22. Crona, M. Ph.D. thesis, Stockholm University (2010).
23. Torrents, E., Westman, M., Sahlin, M. & Sjöberg, B.M. *J. Biol. Chem.* **281**, 25287–25296 (2006).

Glutamate receptor ion channels: where do all the calories go?

Mark L Mayer

Glutamate receptor ion channels use the free energy of ligand binding to trigger ion channel activation and desensitization. In this issue, an analysis of all-atom molecular dynamics simulations dissects the binding process, reveals a substantial gain in free energy produced by domain closure for agonists and reports unique energy landscapes for individual ligands.

Glutamate receptor ion channels (iGluRs) are complex allosteric proteins that have generated enormous interest in the neuroscience community because of their role in synaptic transmission, learning, memory formation and brain development[1]. The emergence of a comprehensive iGluR pharmacology in the 1980s, combined with the cloning of 18 iGluR genes 10 years later, led to the identification of numerous subtype-selective ligands and allosteric modulators. Current medicinal chemistry research programs in the pharmaceutical industry continue to develop new iGluR ligands, several of which have therapeutic potential for a range of neurological and psychiatric diseases. Questions not answered by these studies include what the precise mechanisms underlying the affinity of ligand binding may be and why 'partial agonists' produce less activation than 'full agonists' such as the neurotransmitter glutamate[2,3].

On page 283 of this issue, Lau and Roux[4] use a comprehensive set of all-atom molecular dynamics simulations for a panel of nine iGluR agonists, partial agonists and antagonists to address these and other important problems in the binding-gating conundrum for ligand-activated ion channels. Using this approach, they dissect the energetics of binding into components resulting from ligand interactions with the protein, on the one hand, from the free-energy changes resulting from ligand-induced conformational modifications on the other. Surprisingly, they find that the binding of glutamate is energetically unfavorable when it is docked into the ligand-binding domain (LBD), but this is compensated for by a large free-energy change produced by closure of the LBD (**Fig. 1**). They find that the energy resulting from LBD closure is less for partial agonists than for full agonists, but there are unique landscapes for each of the nine ligands studied, highlighting the complexity of mechanisms that underlie the binding of small molecules to proteins. Such a comprehensive analysis of the energetics of ligand binding to a neurotransmitter receptor has not been attempted before. It will undoubtedly be applied to other systems when crystal structures have been solved to provide the necessary molecular templates for molecular dynamics simulations.

Lau and Roux study the α-amino-3-hydroxy-5-methyl-4-isoxazolepropionic acid (AMPA) receptor GluA2, a model system for the receptor family that mediates fast synaptic transmission throughout the brain, and the only iGluR for which a full-length structure has been solved[5]. By contrast, during the past decade, numerous biochemical, crystallographic and NMR studies have focused on the LBDs of iGluRs, which can be genetically isolated and expressed as soluble recombinant proteins. GluA2, in particular, has been studied extensively, and more than 80 ligand complexes have been solved by X-ray crystallography[6]. These studies have generated models for activation[7] and desensitization[8] that have been amply substantiated by experimental tests[9–12] and have also identified binding sites for allosteric modulators[8,13,14]. Despite these impressive advances, our understanding of the

Mark L. Mayer is at the Laboratory of Cellular and Molecular Neurophysiology, Porter Neuroscience Research Center, National Institute of Child Health and Human Development, National Institutes of Health, Bethesda, Maryland, USA.
e-mail: mayerm@mail.nih.gov

thermodynamic principles that underlie binding of glutamate receptor ligands has remained primitive. Although molecular dynamics simulations have previously been done for the LBDs of iGluRs[15,16], these have largely ignored the energetics of ligand binding. The results of Lau and Roux represent a radical departure from this and suggest that the trajectory from the open to the closed conformation of the LBD differs for individual ligands, even when the end states are similar; the trajectory for binding of glutamate reveals at least two intermediate structures (**Fig. 1**). Also striking is the difference in conformational stability of the 6,7-dinitroquinoxaline-2,3-dione (CNQX) and 6-cyano-7-nitroquinoxaline-2,3-dione (DNQX) complexes, antagonists that are generally considered as having nearly identical binding mechanisms.

Lau and Roux then go on to assemble an LBD tetramer, based on the full-length GluA2 crystal structure[5], and they compare the root-mean-square (r.m.s.) deviation fluctuations for individual ligand complexes taken from their simulations with those calculated for crystal structures of the isolated LBD. One notable result is that for some partial agonists, the dimer pairs that make up a tetramer assembly undergo different degrees of movement, producing subunit nonequivalence in the gating mechanism. This is a surprising finding that has experimental precedent from work on kainate-subtype iGluRs[17]. For some ligands, notably the partial agonist kainate and the antagonist CNQX, which also acts as a very weak partial agonist in native AMPA receptors[18], there is a 4–6 Å reduction in average r.m.s. deviation in the simulated tetramer assembly, compared to the isolated LBD crystal structures; however, for the AMPA-bound, 2-amino-3-[5-*tert*-butyl-3-(phosphonomethoxy)-4-isoxazolyl]propionic acid (ATPO)-bound and apo structures, the opposite is true. These differences seem to arise from the unique conformational ensembles computed for the various ligand complexes.

Although studies like that undertaken by Lau and Roux are badly needed in order to understand in molecular detail how binding of neurotransmitters activates ligand-gated ion channels, there are caveats to the approach. The force fields for all-atom molecular dynamics simulations have now been validated—albeit imperfectly—in numerous simulations, so we can probably cross that off our list of concerns. The simulations were done using isolated LBDs, the same as used for structural and biochemical studies; however, in the intact receptor, each of the four LBDs is coupled at one end to a large N-terminal domain, which itself assembles as a dimer of dimers, and is attached at the other end by three connections to the ion-channel segment. Also different from the intact receptor, in which each of the four LBDs is packed against its partners in a dimer-of-dimers assembly, are intersubunit interactions mediated by essential structural elements directly involved in either ligand binding or the conformational change induced by agonists and partial agonists. How serious is this? One answer would be that the results shed light on the amount of energy available for ion channel gating, but in the intact receptor, the energy profile of the reaction coordinate leading from the open to the closed state may differ from that seen in the isolated LBD. Any information about how the binding energy of agonists drives the process of desensitization is also absent.

Despite these limitations, the study by Lau and Roux provides refreshing new insights into the energetics of iGluR activation, which will doubtless spur calculations for intact iGluR assemblies. Computational studies for other iGluR LBDs will be equally interesting, particularly studies of the glycine-binding subunits of NMDA receptors, for which several partial agonist crystal structures have been solved. Notably, for all of these, the extent of domain closure is nearly identical to that for full agonists[3]. This is strikingly different from what has been found for the large majority of AMPA- and kainate-receptor partial-agonist crystal structures, which reveal intermediate extents of domain closure[2,19,20].

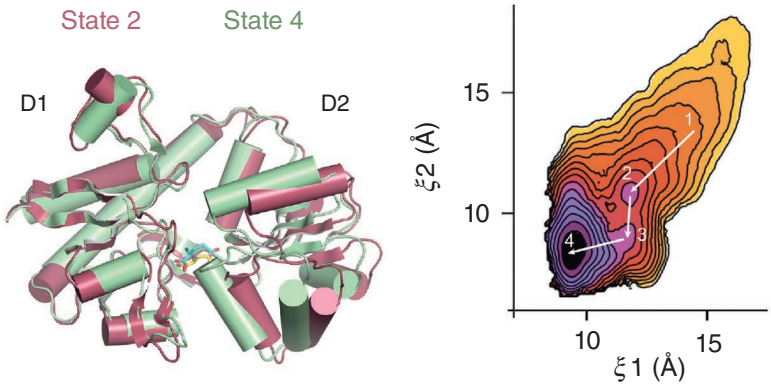

Figure 1 Free-energy changes revealed by molecular dynamics simulations for the GluA2 LBD. The left panel shows ribbon diagrams for glutamate-bound complexes corresponding to state 2, a glutamate-bound intermediate on the open-cleft-to-closed-cleft pathway, and to state 4, the final closed-cleft conformation represented by the crystal structure PDB 1FTJ(ref. 7). The structures were superimposed using domain 1 (D1) coordinates (r.m.s. deviation 0.63 Å for 122 Cα atoms); owing to partial domain closure, the r.m.s. deviation for domain 2 was 4.2 Å (107 Cα atoms), which decreased to 0.8 Å when domain 2 (D2) was independently superimposed on the crystal structure. The energy landscape corresponding to the transition from the open-cleft (state 1) to closed-cleft (state 4) glutamate-bound structures is shown in the right panel. As noted by Lau and Roux[4], the likely pathway for domain closure passes through at least two low-energy intermediates. In state 2, although the ligand makes multiple contacts with atoms in both domains 1 and 2, the pattern of the interactions differs from that in the fully closed conformation. In addition, important interdomain contacts—for example, the hydrogen bond between the side chains of Glu402 and Thr685—are not yet established in state 2. This is because Thr685 in α-helix H moves an additional 6 Å toward domain 1 in the transition from state 2 to state 4, highlighting the role of cleft closure in contributing energy to the glutamate-bound complex.

COMPETING FINANCIAL INTERESTS
The author declares no competing financial interests.

1. Traynelis, S.F. *et al. Pharmacol. Rev.* **62**, 405–496 (2010).
2. Jin, R., Banke, T.G., Mayer, M.L., Traynelis, S.F. & Gouaux, E. *Nat. Neurosci.* **6**, 803–810 (2003).
3. Inanobe, A., Furukawa, H. & Gouaux, E. *Neuron* **47**, 71–84 (2005).
4. Lau, A.Y. & Roux, B. *Nat. Struct. Mol. Biol.* **18**, 283–287 (2011).
5. Sobolevsky, A.I., Rosconi, M.P. & Gouaux, E. *Nature* **462**, 745–756 (2009).
6. Pøhlsgaard, J., Frydenvang, K., Madsen, U. & Kastrup, J.S. *Neuropharmacology* **60**, 135–150 (2011).
7. Armstrong, N. & Gouaux, E. *Neuron* **28**, 165–181 (2000).
8. Sun, Y. *et al. Nature* **417**, 245–253 (2002).
9. Horning, M.S. & Mayer, M.L. *Neuron* **41**, 379–388 (2004).
10. Weston, M.C., Schuck, P., Ghosal, A., Rosenmund, C. & Mayer, M.L. *Nat. Struct. Mol. Biol.* **13**, 1120–1127 (2006).
11. Zhang, W., Cho, Y., Lolis, E. & Howe, J.R. *J. Neurosci.* **28**, 932–943 (2008).
12. Chaudhry, C., Weston, M.C., Schuck, P., Rosenmund, C. & Mayer, M.L. *EMBO J.* **28**, 1518–1530 (2009).
13. Jin, R. *et al. J. Neurosci.* **25**, 9027–9036 (2005).
14. Ahmed, A.H., Ptak, C.P. & Oswald, R.E. *Biochemistry* **49**, 2843–2850 (2010).
15. Arinaminpathy, Y., Sansom, M.S. & Biggin, P.C. *Mol. Pharmacol.* **69**, 11–18 (2006).
16. Kaye, S.L., Sansom, M.S. & Biggin, P.C. *J. Biol. Chem.* **281**, 12736–12742 (2006).
17. Das, U., Kumar, J., Mayer, M.L. & Plested, A.J. *Proc. Natl. Acad. Sci. USA* **107**, 8463–8468 (2010).
18. Menuz, K., Stroud, R.M., Nicoll, R.A. & Hays, F.A. *Science* **318**, 815–817 (2007).
19. Mayer, M.L. *Neuron* **45**, 539–552 (2005).
20. Hald, H. *et al. J. Biol. Chem.* **282**, 25726–25736 (2007).

Supplementary Information

The Hidden Energetics of Ligand Binding and Activation in a Glutamate Receptor

Albert Y. Lau[1,2] and Benoît Roux[1]

[1]Department of Biochemistry and Molecular Biology
The University of Chicago, Chicago, IL 60637, USA

[2]Present address: Department of Biophysics and Biophysical Chemistry
Johns Hopkins University School of Medicine, Baltimore, MD 21205, USA

Correspondence should be addressed to Benoît Roux: roux@uchicago.edu

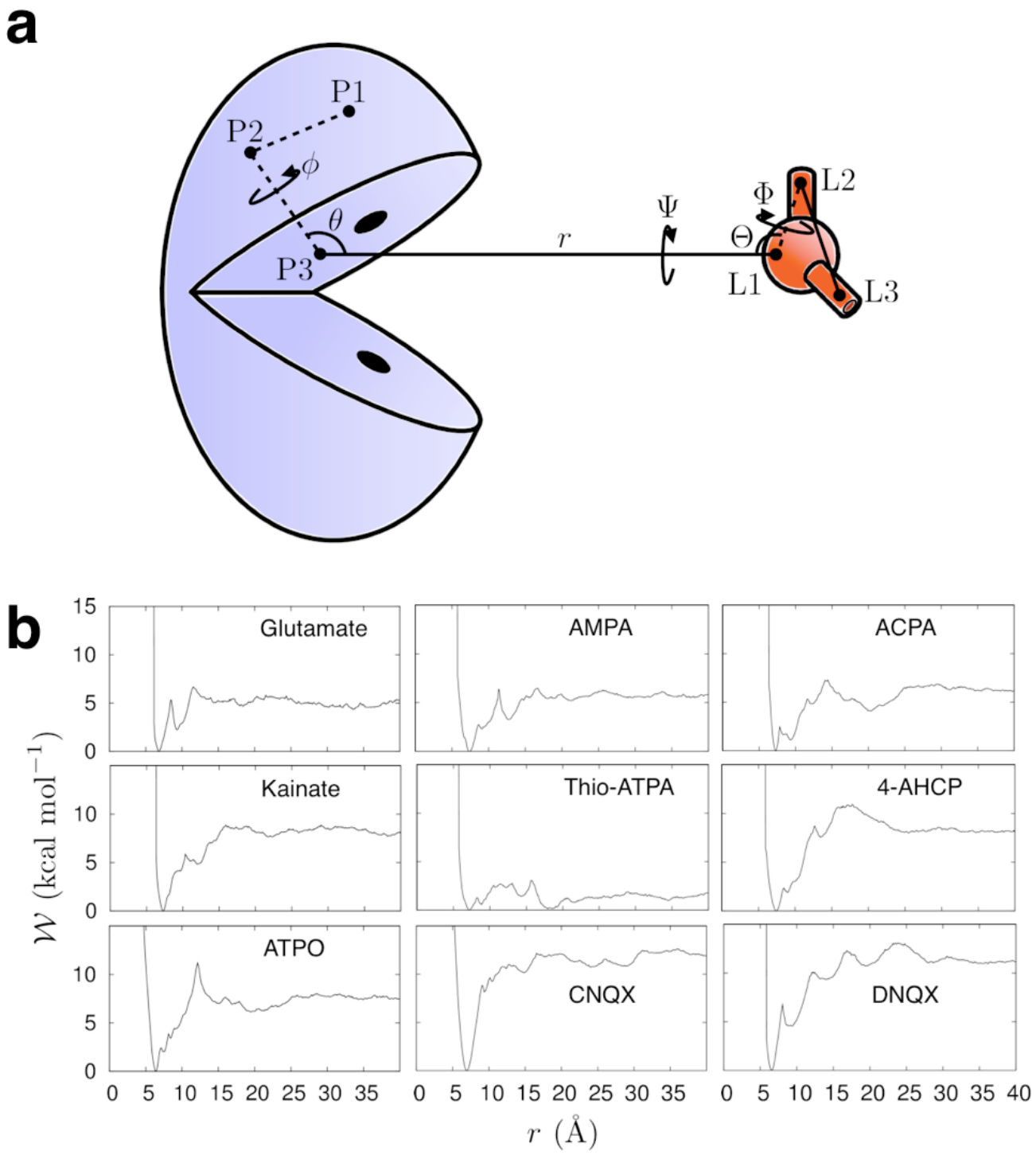

Supplementary Figure 1. Ligand docking. (**a**) Schematic diagram describing the position (r, θ, ϕ) and orientation (Θ, Φ, Ψ) of the ligand relative to the receptor protein. For the position, the P3–L1 distance is r, the P2–P3–L1 angle is θ, and the P1–P2–P3–L1 dihedral angle is ϕ. For the orientation, the P3–L1–L2 angle is Θ, the P3–L1–L2–L3 dihedral angle is Φ, and the P2–P3–L1–L2 dihedral angle is Ψ. (**b**) The computed PMF $\mathcal{W}(r)$, where r is the distance between the center-of-mass of the ligand and the protein docking site. The reference distance r^* is 40 Å.

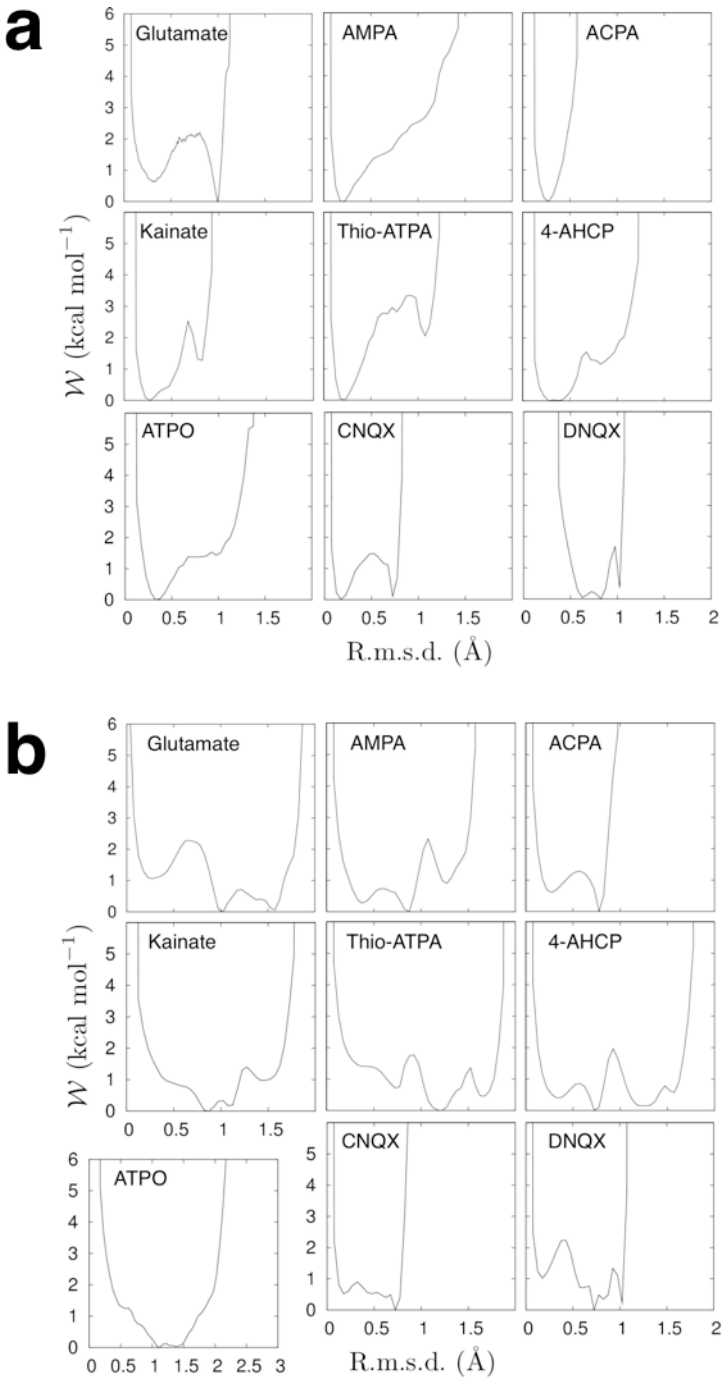

Supplementary Figure 2. The computed PMF of the ligand conformational degrees of freedom as a function of the r.m.s.d. (**a**) The ligand is inserted into the open LBD docking site. (**b**) The ligand is in the bulk. The PMF for ATPO is plotted on a different scale from the others.

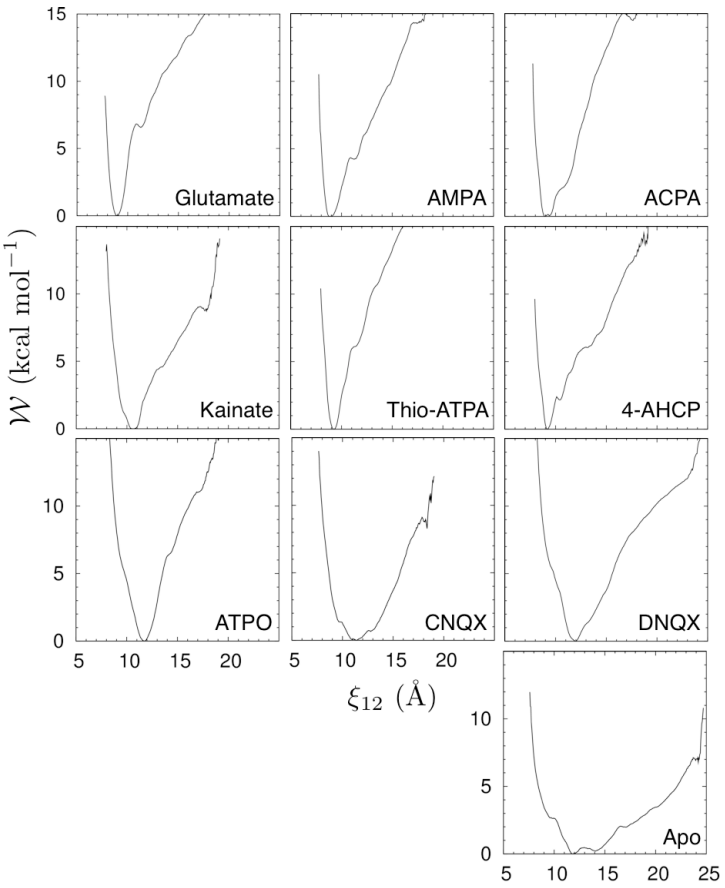

Supplementary Figure 3. 1D coordinate projection, $\xi_{12} = (\xi_1 + \xi_2)/2$, of the 2D free energy landscapes $\mathcal{W}(\xi_1, \xi_2)$ (see **Fig. 2**).

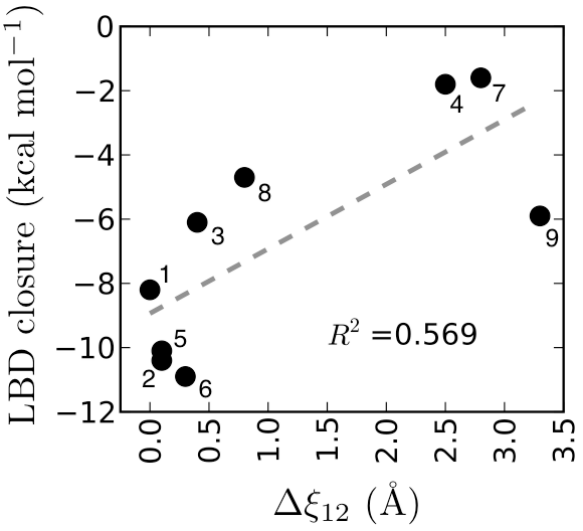

Supplementary Figure 4. The calculated $\Delta G_{\mathrm{close}}$ vs. the relative amount of LBD closure observed in each LBD–ligand crystal structure. $\Delta\xi_{12}$ is measured relative to the LBD–AMPA structure, where $\xi_{12} = (\xi_1 + \xi_2)/2$. The correlation coefficient is reported for a linear regression fit to the data, shown as a dashed line. 1 = AMPA, 2 = ACPA, 3 = 4-AHCP, 4 = CNQX, 5 = glutamate, 6 = thio-ATPA, 7 = DNQX, 8 = kainate, and 9 = ATPO.

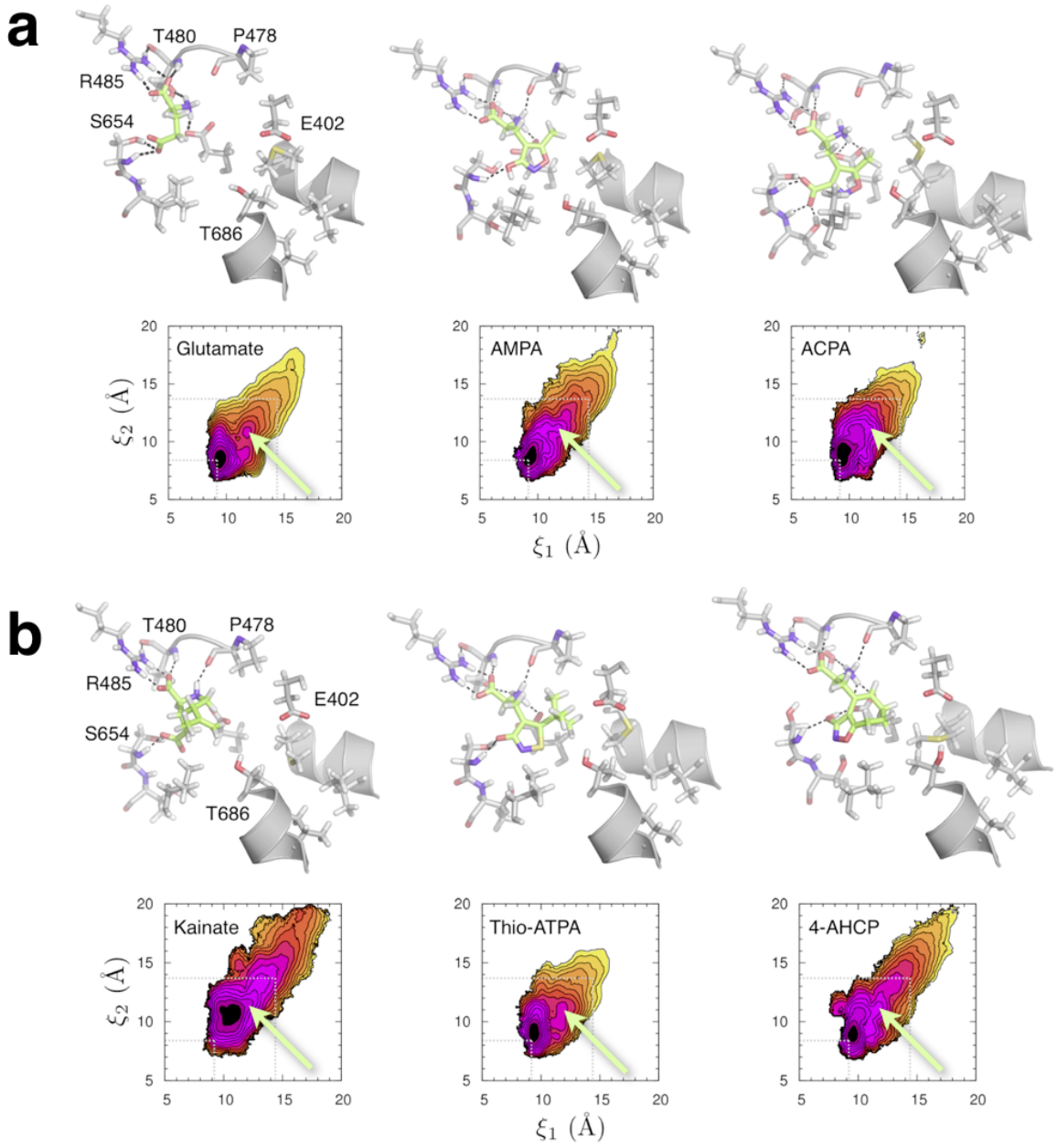

Supplementary Figure 5. Interactions between ligands and residues in the LBD binding site corresponding to the conformation indicated by the arrow. Full agonists are shown in (**a**), and partial agonists are shown in (**b**).

Component	Glutamate	AMPA	ACPA
$\Delta G_{\mathrm{c,site}}$ (kcal mol^{-1})	0.34	0.10	0.08
$\Delta G_{\mathrm{c,bulk}}$ (kcal mol^{-1})	1.05	0.44	0.31
$\Delta G_{\mathrm{o,site}}$ (kcal mol^{-1})	0.41	1.70	0.70
$\Delta G_{\mathrm{o,bulk}}$ (kcal mol^{-1})	4.89	5.07	5.10
$\Delta G_{\mathrm{a,site}}$ (kcal mol^{-1})	0.65	1.44	1.10
$\Delta G_{\mathrm{p,site}}$ (kcal mol^{-1})	12.46	10.60	12.69
$\Delta G_{\mathrm{p,bulk}}$ (kcal mol^{-1})	2.33	2.33	2.33
S^* (Å^2)	126.94	117.67	129.31
I^* (Å)	4.53×10^3	1.44×10^4	1.97×10^4
$\Delta G^{(\circ)}_{\mathrm{dock}}$ (kcal mol^{-1})	1.05	-1.86	-0.85
$\Delta G_{\mathrm{close}}$ (kcal mol^{-1})	-10.13	-8.27	-10.36
$\Delta G^{(\circ)}_{\mathrm{bind}}$ (kcal mol^{-1})	-9.08	-10.14	-11.21
Exp. ΔG_{bind} (kcal mol^{-1})	-8.4 (IC$_{50}$)[1]	-10.8 (K_{d})[2]	-10.6 (IC$_{50}$)[2]
Component	Kainate	Thio-ATPA	4-AHCP
$\Delta G_{\mathrm{c,site}}$ (kcal mol^{-1})	0.14	0.08	0.18
$\Delta G_{\mathrm{c,bulk}}$ (kcal mol^{-1})	0.74	1.08	0.66
$\Delta G_{\mathrm{o,site}}$ (kcal mol^{-1})	0.25	0.44	1.28
$\Delta G_{\mathrm{o,bulk}}$ (kcal mol^{-1})	4.85	4.86	4.88
$\Delta G_{\mathrm{a,site}}$ (kcal mol^{-1})	0.53	0.77	0.95
$\Delta G_{\mathrm{p,site}}$ (kcal mol^{-1})	7.02	13.32	8.44
$\Delta G_{\mathrm{p,bulk}}$ (kcal mol^{-1})	2.33	2.33	2.33
S^* (Å^2)	109.65	141.76	144.30
I^* (Å)	4.44×10^5	1.05×10^2	6.44×10^5
$\Delta G^{(\circ)}_{\mathrm{dock}}$ (kcal mol^{-1})	-1.47	3.35	-3.39
$\Delta G_{\mathrm{close}}$ (kcal mol^{-1})	-4.70	-10.99	-6.11
$\Delta G^{(\circ)}_{\mathrm{bind}}$ (kcal mol^{-1})	-6.16	-7.64	-9.50
Exp. ΔG_{bind} (kcal mol^{-1})	-6.6 (IC$_{50}$)[1]	-8.3 (K_{i})[3]	-9.2 (K_{i})[4]
Component	ATPO	CNQX	DNQX
$\Delta G_{\mathrm{c,site}}$ (kcal mol^{-1})	0.21	0.16	0.54
$\Delta G_{\mathrm{c,bulk}}$ (kcal mol^{-1})	1.23	0.27	0.50
$\Delta G_{\mathrm{o,site}}$ (kcal mol^{-1})	0.39	0.31	0.71
$\Delta G_{\mathrm{o,bulk}}$ (kcal mol^{-1})	4.83	4.81	4.78
$\Delta G_{\mathrm{a,site}}$ (kcal mol^{-1})	0.69	0.45	0.98
$\Delta G_{\mathrm{p,site}}$ (kcal mol^{-1})	8.23	4.07	3.93
$\Delta G_{\mathrm{p,bulk}}$ (kcal mol^{-1})	2.33	2.33	2.33
S^* (Å^2)	146.23	137.20	132.27
I^* (Å)	1.32×10^5	2.88×10^8	7.59×10^7
$\Delta G^{(\circ)}_{\mathrm{dock}}$ (kcal mol^{-1})	-0.81	-5.98	-6.26
$\Delta G_{\mathrm{close}}$ (kcal mol^{-1})	-5.91	-1.74	-1.60
$\Delta G^{(\circ)}_{\mathrm{bind}}$ (kcal mol^{-1})	-6.72	-7.73	-7.86
Exp. ΔG_{bind} (kcal mol^{-1})	-6.6 (IC$_{50}$)[5]	-8.5 (IC$_{50}$)[6]	-8.2 (IC$_{50}$)[1]

Supplementary Table 1. Components of the absolute binding free energy for each ligand.

Ligand	$\Delta\Delta G_{\mathrm{ion}}$ (kcal mol^{-1})
glutamate	-3.1
AMPA	3.2
thio-ATPA	-2.1
4-AHCP	0.7

Supplementary Table 2. Free energy of ionizing a ligand when transferring it from bulk solvent into a closed LBD. Each value is an average of forward and backward FEP calculations.

Component	AMPA	4-AHCP
$\Delta G_{\mathrm{c,site}}$ (kcal mol^{-1})	0.12	0.12
$\Delta G_{\mathrm{c,bulk}}$ (kcal mol^{-1})	0.66	0.57
$\Delta G_{\mathrm{o,site}}$ (kcal mol^{-1})	0.42	2.83
$\Delta G_{\mathrm{o,bulk}}$ (kcal mol^{-1})	5.07	4.88
$\Delta G_{\mathrm{a,site}}$ (kcal mol^{-1})	0.69	1.02
$\Delta G_{\mathrm{p,site}}$ (kcal mol^{-1})	10.11	10.36
$\Delta G_{\mathrm{p,bulk}}$ (kcal mol^{-1})	2.33	2.33
S^* (Å^2)	117.67	144.30
I^* (Å)	3.97×10^4	4.28×10^7
$\Delta G^{(\circ)}_{\mathrm{dock}}$ (kcal mol^{-1})	-0.25	-7.54
$\Delta G_{\mathrm{close}}$ (kcal mol^{-1})	-7.78	-8.03
$\Delta G^{(\circ)}_{\mathrm{bind}}$ (kcal mol^{-1})	-8.03	-15.57
Exp. ΔG_{bind} (kcal mol^{-1})	-10.8 (K_{d})[2]	-9.2 (K_{i})[4]

Supplementary Table 3. Components of the absolute binding free energy for AMPA and 4-AHCP in an alternate ionization state (ionized 3-hydroxy group of the isoxazole ring; total charge of -1).

Ligand[a]	Free Energy Min.[b]	Cryst. Conf.[b]	PDB ID
Full Agonists			
Glutamate (-1)	(9.4, 8.4), 8.9	(9.5, 7.8), 8.7	1FTJ
AMPA (0)	(9.2, 8.4), 8.8	(9.3, 7.8), 8.6	1FTM
ACPA (-1)	(9.4, 8.4), 8.9	(9.3, 8.0), 8.7	1M5E
Partial Agonists			
Kainate (-1)	(10.9, 10.6), 10.8	(9.7, 9.2), 9.4	1FTK
Thio-ATPA (-1)	(9.4, 9.0), 9.2	(9.5, 8.4), 8.9	2AIX
4-AHCP (0)	(9.6, 8.9), 9.3	(9.5, 8.5), 9.0	1WVJ
Antagonists			
ATPO (-1)	(11.9, 11.5), 11.7	(12.3, 11.6), 11.9	1N0T
CNQX (0)	(11.5, 11.3), 11.4	(11.5, 10.6), 11.1	3B7D
DNQX (0)	(12.7, 11.3), 12.0	(12.0, 10.8), 11.4	1FTL

[a] The total charge of the ligand is indicated in parentheses.
[b] (ξ_1, ξ_2) and ($\xi_1 + \xi_2$)/2 are given in units of Å.

Supplementary Table 4. Closure of the GluA2 LBD. For each LBD–ligand complex, the location of the computed free energy minimum and the crystal structure conformation are compared.

Measurement	Glutamate	AMPA	ACPA	
R.m.s.d. (Å)	30.9 (4.0), 31.5	36.7 (4.4), 33.1	35.2 (4.8), 34.4	
A–D (Å)	39.8 (3.2), 39.0	41.9 (2.4), 39.6	41.3 (2.0), 40.0	
B–C (Å)	39.9 (3.2), 39.1	41.9 (2.6), 39.7	41.3 (2.2), 40.0	
A–B (Å)	42.3 (1.6), 42.2	42.9 (1.6), 42.6	42.9 (1.4), 43.0	
C–D (Å)	45.2 (1.8), 45.3	46.0 (1.8), 45.6	45.9 (1.4), 46.0	
A–C (Å)	29.5 (2.6), 31.7	30.6 (2.0), 31.5	29.9 (3.0), 30.8	
B–D (Å)	74.2 (3.0), 72.9	76.5 (2.6), 73.9	76.1 (1.8), 74.9	
Measurement	Kainate	Thio-ATPA	4-AHCP	
R.m.s.d. (Å)	17.3 (5.4), 21.0	30.8 (3.0), 29.1	26.7 (4.6), 27.6	
A–D (Å)	34.3 (2.8), 34.2	39.5 (2.4), 38.0	37.9 (2.4), 37.1	
B–C (Å)	34.4 (3.0), 34.2	39.5 (2.2), 38.1	37.9 (2.2), 37.2	
A–B (Å)	40.9 (2.0), 42.4	42.4 (1.6), 42.4	41.9 (1.6), 42.3	
C–D (Å)	43.4 (2.0), 44.7	45.2 (1.6), 45.2	44.6 (1.4), 45.1	
A–C (Å)	25.9 (2.6), 25.2	28.6 (2.2), 29.5	28.4 (2.6), 29.4	
B–D (Å)	68.9 (3.2), 70.7	74.3 (2.2), 72.9	72.4 (2.4), 72.0	
Measurement	ATPO	CNQX	DNQX	Apo
R.m.s.d. (Å)	12.7 (4.0), 8.6	12.5 (4.6), 15.9	11.4 (4.4), 12.1	12.7 (5.4), 7.8
A–D (Å)	32.4 (2.8), 30.3	32.5 (4.2), 33.6	30.7 (3.8), 32.1	27.3 (7.4), 30.4
B–C (Å)	32.5 (2.8), 30.3	32.5 (4.0), 33.6	30.8 (4.0), 32.1	27.4 (7.8), 30.4
A–B (Å)	40.5 (2.0), 39.9	40.5 (2.4), 41.1	39.7 (2.4), 40.7	39.2 (4.2), 40.1
C–D (Å)	42.7 (2.0), 42.2	42.7 (2.4), 43.5	41.8 (2.4), 42.9	41.1 (4.2), 42.2
A–C (Å)	23.9 (2.8), 26.2	24.5 (3.0), 26.3	25.1 (2.6), 25.9	24.1 (3.8), 25.5
B–D (Å)	67.3 (2.8), 64.4	67.1 (4.0), 68.4	64.7 (3.4), 66.8	61.7 (6.6), 64.8

Supplementary Table 5. LBD conformational distributions in the context of an intact receptor. LBD–ligand complexes were superimposed onto Lobe 1 of each LBD in the intact GluA2 crystal structure. The r.m.s.d. and inter-subunit distances were measured in Lobe 2. The r.m.s.d. refers to the average value measured between each LBD–ligand tetrameric assembly and the intact GluA2 structure (see **Fig. 4**), with the full width at half max (FWHM) in parentheses, and the value measured between the crystal structure of each LBD–ligand complex and the intact GluA2 structure after the comma. For each inter-subunit pair, the average distance $\langle d \rangle$ is reported, with the FWHM in parentheses (see **Fig. 5**), and the distance d measured between the crystal structure of each LBD–ligand complex superimposed onto the intact GluA2 crystal structure after the comma.

SUPPLEMENTARY METHODS

Ligand conformational PMF, $\mathcal{W}(\zeta)$

The conformational PMF $\mathcal{W}(\zeta)$ was computed for the ligand when it is either inserted into the docking site or when it is in the bulk, using umbrella sampling simulations, where ζ is the r.m.s.d. of the ligand relative to its average conformation in the docked state (see **Supplementary Fig. 2**). The atom selection included all non-hydrogen atoms. The conformation of the ligand was restrained using a harmonic potential with a force constant of 1 kcal mol^{-1} Å^{-2}. Each PMF was computed from either 9 or 17 umbrella windows spaced 0.25 Å apart. The free energies $\Delta G_{\mathrm{c,site}}$ and $\Delta G_{\mathrm{c,bulk}}$ are calculated as follows:

$$e^{-\beta \Delta G_{\mathrm{c,site}}} = \frac{\int d\zeta \; e^{-\beta[\mathcal{W}_{\mathrm{c,site}}(\zeta)+u_{\mathrm{c}}(\zeta)]}}{\int d\zeta \; e^{-\beta \mathcal{W}_{\mathrm{c,site}}(\zeta)}} \tag{1a}$$

$$e^{-\beta \Delta G_{\mathrm{c,bulk}}} = \frac{\int d\zeta \; e^{-\beta[\mathcal{W}_{\mathrm{c,bulk}}(\zeta)+u_{\mathrm{c}}(\zeta)]}}{\int d\zeta \; e^{-\beta \mathcal{W}_{\mathrm{c,bulk}}(\zeta)}}. \tag{1b}$$

The number of atoms in the "site" system is ∼46,000 (86 Å × 80 Å × 70 Å), and the total simulation time for each PMF is ∼1 ns. The number of atoms in the "bulk" simulation system is ∼1,400 (24 Å × 24 Å × 24 Å), and the total simulation time for each PMF is ∼5 ns.

Ligand orientational and axial free energies

The free energies $\Delta G_{\mathrm{o,site}}$ and $\Delta G_{\mathrm{a,site}}$ were calculated from **Supplementary Eqs. 4c,d** using free energy perturbation (FEP) with 10 intermediate values of the thermodynamic coupling parameter λ between 0 and 1. The orientation of the ligand was restrained using the harmonic potential $u_{\mathrm{o}}(\Theta, \Phi, \Psi) = k_{\mathrm{o}}[(\Theta - \Theta_{\mathrm{ref}})^2 + (\Phi - \Phi_{\mathrm{ref}})^2 + (\Psi - \Psi_{\mathrm{ref}})^2]$, where the reference is the average orientation of the docked ligand, and k_{o} = 40 kcal mol^{-1} rad^{-2}. The axial restraint is $u_{\mathrm{a}}(\theta, \phi) = k_{\mathrm{a}}[(\theta - \theta_{\mathrm{ref}})^2 + (\phi - \phi_{\mathrm{ref}})^2]$, where the reference is the average value for the docked ligand, and k_{a} = 40 kcal mol^{-1} rad^{-2}. The number of atoms in the system is ∼46,000 (86 Å × 80 Å × 70 Å), and the total simulation time is ∼1 ns. $\Delta G_{\mathrm{o,bulk}}$ was calculated from **Supplementary Eq. 4e** by direct numerical integration over the three Euler angles. The surface element S^* was calculated by direct numerical integration of **Supplementary Eq. 8**. The LBD reference frame is defined by the center-of-mass of the following residues (see **Supplementary Fig. 1a**): F491 (P1), L428 (P2), and T480+Y732 (P3).

Ligand ΔpK_a

The protonation states of all ionizable groups of each ligand at neutral pH were determined using the program SPARC[7,8] (http://sparc.chem.uga.edu; see **Fig. 1**), which predicts ionization constants of pharmaceutical compounds using an empirical method. When a ligand docks into an open LBD, the ionizable groups on the ligand distal to R485 of the protein are solvent exposed, so the protonation states of these groups are expected to be the same as the isolated ligand in bulk solvent. LBD closure, however, shields the ligand from solvent, so shifts in $\mathrm{p}K_\mathrm{a}$, and consequently protonation states, are possible. The 3-hydroxy substituent of either the isoxazole or isothiazolol ring of AMPA, thio-ATPA, and 4-AHCP are predicted to have $\mathrm{p}K_\mathrm{a}$ values close to 7 (8.0, 6.4, and 8.5, respectively), and are therefore the groups most likely to change their protonation states.

FEP calculations were performed to determine $\Delta\mathrm{p}K_\mathrm{a}$ for these groups when the ligand is transferred from bulk solvent to the binding site of a closed LBD. The simulation system consists of a closed LBD–ligand complex with a second free ligand molecule in the bulk solvent region. The two ligands are in different protonation states. The free energy difference $\Delta\Delta G$ of transferring a proton from one ligand to the other is computed using 10 intermediate values of the thermodynamic coupling parameter λ between 0 and 1 (see **Supplementary Table 2**). The $\Delta\mathrm{p}K_\mathrm{a}$ between the bound and unbound ligand is $\Delta\mathrm{p}K_\mathrm{a} = -\Delta\Delta G/(2.3\,k_\mathrm{B}T)$[9]. The γ-carboxylate moiety of a glutamate ligand is not expected to become protonated upon binding to the LBD and was evaluated as a control. The number of atoms in the system is ~46,000 (86 Å × 80 Å × 70 Å), and the total simulation time for each calculation is ~200 ps.

MD simulation parameters

All simulations were performed using the program CHARMM[10] with explicit solvent. The all-atom potential-energy function PARAM27 for proteins[11] and the TIP3P potential energy function for water[12] were used. Electrostatic interactions were computed using the particle mesh Ewald (PME) algorithm[13], and short-range, nonbonded interactions were truncated at 10 Å. The SHAKE algorithm[14] was used to constrain bond lengths involving hydrogen atoms. A time step of 2 fs was used. The initial protein configuration of each system was relaxed with Langevin dynamics in the presence of harmonic restraints at constant volume for ~300 ps to avert spurious disruption of the protein structure. The cell dimensions were subsequently allowed to vary in accordance with a constant pressure (1 atm) and temperature (300 K) thermodynamic ensemble[15].

Theory

The equilibrium binding constant $K_{\rm eq}$ can be written as a ratio of configurational integrals representing the initial and final states of the ligand-binding process[16],

$$K_{\rm eq} = \frac{\int_{\rm site} d\mathbf{L} \int d\mathbf{X}\; e^{-\beta U}}{\int_{\rm bulk} d\mathbf{L}\; \delta(\mathbf{r}-\mathbf{r}^*) \int d\mathbf{X}\; e^{-\beta U}}. \tag{2}$$

The denominator is an integral over the degrees of freedom of the system when a single ligand molecule is in the bulk solvent region (initial state). The numerator is the corresponding integral when the ligand occupies the binding site of the protein receptor (final state). $\mathbf{L}$ is the degrees of freedom of the ligand, and $\mathbf{X}$ is the degrees of freedom of the receptor and solvent. $\mathbf{r}$ is the position of the ligand relative to the receptor, and $\mathbf{r}^*$ is an arbitrarily specified position in the bulk, far away from the receptor. U is the total potential energy of the system, and $1/\beta = k_{\rm B}T$ is the Boltzmann constant times temperature. The position of the center-of-mass of the ligand relative to the receptor can be specified by (r, θ, ϕ) in spherical coordinates, and the orientation of the ligand relative to the receptor can be specified by the Euler angles (Θ, Φ, Ψ) (see **Supplementary Fig. 1a** for a schematic diagram).

$K_{\rm eq}$ can be expanded into a product of configurational integrals that include applied restraining potentials, which limit the configurational space that must be sampled,

$$\begin{aligned} K_{\rm eq} = {} & \frac{\int_{\rm site} d\mathbf{L} \int d\mathbf{X}\; e^{-\beta U}}{\int_{\rm site} d\mathbf{L} \int d\mathbf{X}\; e^{-\beta[U+u_{\rm p}]}} \times \frac{\int_{\rm site} d\mathbf{L} \int d\mathbf{X}\; e^{-\beta[U+u_{\rm p}]}}{\int_{\rm site} d\mathbf{L} \int d\mathbf{X}\; e^{-\beta[U+u_{\rm p}+u_{\rm c}]}} \times \frac{\int_{\rm site} d\mathbf{L} \int d\mathbf{X}\; e^{-\beta[U+u_{\rm p}+u_{\rm c}]}}{\int_{\rm site} d\mathbf{L} \int d\mathbf{X}\; e^{-\beta[U+u_{\rm p}+u_{\rm c}+u_{\rm o}]}} \\ & \times \frac{\int_{\rm site} d\mathbf{L} \int d\mathbf{X}\; e^{-\beta[U+u_{\rm p}+u_{\rm c}+u_{\rm o}]}}{\int_{\rm site} d\mathbf{L} \int d\mathbf{X}\; e^{-\beta[U+u_{\rm p}+u_{\rm c}+u_{\rm o}+u_{\rm a}]}} \times \frac{\int_{\rm site} d\mathbf{L} \int d\mathbf{X}\; e^{-\beta[U+u_{\rm p}+u_{\rm c}+u_{\rm o}+u_{\rm a}]}}{\int_{\rm bulk} d\mathbf{L}\; \delta(\mathbf{r}-\mathbf{r}^*) \int d\mathbf{X}\; e^{-\beta[U+u_{\rm p}+u_{\rm c}+u_{\rm o}]}} \\ & \times \frac{\int_{\rm bulk} d\mathbf{L}\; \delta(\mathbf{r}-\mathbf{r}^*) \int d\mathbf{X}\; e^{-\beta[U+u_{\rm p}+u_{\rm c}+u_{\rm o}]}}{\int_{\rm bulk} d\mathbf{L}\; \delta(\mathbf{r}-\mathbf{r}^*) \int d\mathbf{X}\; e^{-\beta[U+u_{\rm p}+u_{\rm c}]}} \times \frac{\int_{\rm bulk} d\mathbf{L}\; \delta(\mathbf{r}-\mathbf{r}^*) \int d\mathbf{X}\; e^{-\beta[U+u_{\rm p}+u_{\rm c}]}}{\int_{\rm bulk} d\mathbf{L}\; \delta(\mathbf{r}-\mathbf{r}^*) \int d\mathbf{X}\; e^{-\beta[U+u_{\rm p}]}} \\ & \times \frac{\int_{\rm bulk} d\mathbf{L}\; \delta(\mathbf{r}-\mathbf{r}^*) \int d\mathbf{X}\; e^{-\beta[U+u_{\rm p}]}}{\int_{\rm bulk} d\mathbf{L}\; \delta(\mathbf{r}-\mathbf{r}^*) \int d\mathbf{X}\; e^{-\beta U}}. \end{aligned} \tag{3}$$

The restraining potentials are chosen to be appropriate for the binding of a flexible ligand to a flexible receptor. The potential $u_{\rm p}(\xi)$ restrains the large conformational transitions of the receptor, $u_{\rm c}(\zeta)$ restrains the conformation of the ligand, $u_{\rm o}(\Theta, \Phi, \Psi)$ restrains the orientation of the ligand relative to the receptor, and $u_{\rm a}(\theta, \phi)$ restrains the axial position of the ligand relative to the receptor.

In **Supplementary Eq. 3**, all terms except the fifth one can be written as a free energy difference,

$$e^{-\beta\Delta G_{\mathrm{p,site}}} = \frac{\int_{\mathrm{site}} d\mathbf{L} \int d\mathbf{X}\; e^{-\beta[U+u_{\mathrm{p}}]}}{\int_{\mathrm{site}} d\mathbf{L} \int d\mathbf{X}\; e^{-\beta U}} = \left\langle e^{-\beta u_{\mathrm{p}}} \right\rangle_{(\mathrm{site},\, U)} \tag{4a}$$

$$e^{-\beta\Delta G_{\mathrm{c,site}}} = \frac{\int_{\mathrm{site}} d\mathbf{L} \int d\mathbf{X}\; e^{-\beta[U+u_{\mathrm{p}}+u_{\mathrm{c}}]}}{\int_{\mathrm{site}} d\mathbf{L} \int d\mathbf{X}\; e^{-\beta[U+u_{\mathrm{p}}]}} = \left\langle e^{-\beta u_{\mathrm{c}}} \right\rangle_{(\mathrm{site},\, U+u_{\mathrm{p}})} \tag{4b}$$

$$e^{-\beta\Delta G_{\mathrm{o,site}}} = \frac{\int_{\mathrm{site}} d\mathbf{L} \int d\mathbf{X}\; e^{-\beta[U+u_{\mathrm{p}}+u_{\mathrm{c}}+u_{\mathrm{o}}]}}{\int_{\mathrm{site}} d\mathbf{L} \int d\mathbf{X}\; e^{-\beta[U+u_{\mathrm{p}}+u_{\mathrm{c}}]}} = \left\langle e^{-\beta u_{\mathrm{o}}} \right\rangle_{(\mathrm{site},\, U+u_{\mathrm{p}}+u_{\mathrm{c}})} \tag{4c}$$

$$e^{-\beta\Delta G_{\mathrm{a,site}}} = \frac{\int_{\mathrm{site}} d\mathbf{L} \int d\mathbf{X}\; e^{-\beta[U+u_{\mathrm{p}}+u_{\mathrm{c}}+u_{\mathrm{o}}+u_{\mathrm{a}}]}}{\int_{\mathrm{site}} d\mathbf{L} \int d\mathbf{X}\; e^{-\beta[U+u_{\mathrm{p}}+u_{\mathrm{c}}+u_{\mathrm{o}}]}} = \left\langle e^{-\beta u_{\mathrm{a}}} \right\rangle_{(\mathrm{site},\, U+u_{\mathrm{p}}+u_{\mathrm{c}}+u_{\mathrm{o}})} \tag{4d}$$

$$e^{-\beta\Delta G_{\mathrm{o,bulk}}} = \frac{\int_{\mathrm{bulk}} d\mathbf{L} \int d\mathbf{X}\; e^{-\beta[U+u_{\mathrm{p}}+u_{\mathrm{c}}+u_{\mathrm{o}}]}}{\int_{\mathrm{bulk}} d\mathbf{L} \int d\mathbf{X}\; e^{-\beta[U+u_{\mathrm{p}}+u_{\mathrm{c}}]}} = \left\langle e^{-\beta u_{\mathrm{o}}} \right\rangle_{(\mathrm{bulk},\, U+u_{\mathrm{p}}+u_{\mathrm{c}})} \tag{4e}$$

$$e^{-\beta\Delta G_{\mathrm{c,bulk}}} = \frac{\int_{\mathrm{bulk}} d\mathbf{L} \int d\mathbf{X}\; e^{-\beta[U+u_{\mathrm{p}}+u_{\mathrm{c}}]}}{\int_{\mathrm{bulk}} d\mathbf{L} \int d\mathbf{X}\; e^{-\beta[U+u_{\mathrm{p}}]}} = \left\langle e^{-\beta u_{\mathrm{c}}} \right\rangle_{(\mathrm{bulk},\, U+u_{\mathrm{p}})} \tag{4f}$$

$$e^{-\beta\Delta G_{\mathrm{p,bulk}}} = \frac{\int_{\mathrm{bulk}} d\mathbf{L} \int d\mathbf{X}\; e^{-\beta[U+u_{\mathrm{p}}]}}{\int_{\mathrm{bulk}} d\mathbf{L} \int d\mathbf{X}\; e^{-\beta U}} = \left\langle e^{-\beta u_{\mathrm{p}}} \right\rangle_{(\mathrm{bulk},\, U)}. \tag{4g}$$

These quantities rigorously account for the free energies associated with applying the various restraining potentials when the ligand is in the bulk and then removing them after the ligand has been inserted into the binding site.

Supplementary Eqs. 4a,g can be rewritten in terms of the protein's conformational PMF, $\mathcal{W}(\xi)$, defined as a function of the multi-dimensional order parameter ξ (see **Fig. 2**),

$$e^{-\beta\Delta G_{\mathrm{p,site}}} = \frac{\int d\xi\; e^{-\beta[\mathcal{W}_{\mathrm{p,site}}(\xi)+u_{\mathrm{p}}(\xi)]}}{\int d\xi\; e^{-\beta\mathcal{W}_{\mathrm{p,site}}(\xi)}} \tag{5a}$$

$$e^{-\beta\Delta G_{\mathrm{p,bulk}}} = \frac{\int d\xi\; e^{-\beta[\mathcal{W}_{\mathrm{p,bulk}}(\xi)+u_{\mathrm{p}}(\xi)]}}{\int d\xi\; e^{-\beta\mathcal{W}_{\mathrm{p,bulk}}(\xi)}}. \tag{5b}$$

Next, let us define a function $\rho(\mathbf{r})$,

$$\rho(\mathbf{r}') \equiv \int d\mathbf{L}\ \delta(\mathbf{r}-\mathbf{r}') \int d\mathbf{X}\ e^{-\beta[U+u_{\rm p}+u_{\rm c}+u_{\rm o}]}.$$

For a sufficiently large distance between the ligand and the receptor, $\rho(\mathbf{r}^*) \equiv \rho(r^*,\theta^*,\phi^*)$ becomes independent of θ^* and ϕ^*, i.e., $\rho(\mathbf{r}^*) = \rho(r^*,0,0)$. The fifth term in **Supplementary Eq. 3** can then be written as follows:

$$\begin{aligned}
\frac{\int_{\rm site} d\mathbf{L} \int d\mathbf{X}\ e^{-\beta[U+u_{\rm p}+u_{\rm c}+u_{\rm o}+u_{\rm a}]}}{\int_{\rm bulk} d\mathbf{L}\ \delta(\mathbf{r}-\mathbf{r}^*) \int d\mathbf{X}\ e^{-\beta[U+u_{\rm p}+u_{\rm c}+u_{\rm o}]}} &= \frac{\int_{\rm site} d\mathbf{r}\ \rho(\mathbf{r})\ e^{-\beta u_{\rm a}}}{\rho(\mathbf{r}^*)} \\
&= \frac{\int_{\rm site} d\mathbf{r}\ \rho(\mathbf{r})\ e^{-\beta u_{\rm a}}}{\rho(r^*,0,0)} \\
&= \frac{\int_{\rm site} d\mathbf{r}\ \rho(\mathbf{r})\ e^{-\beta u_{\rm a}}}{\rho(r^*,0,0) \times \frac{\int d\mathbf{r}\ \delta(r-r^*)\ e^{-\beta u_{\rm a}}}{\int d\mathbf{r}\ \delta(r-r^*)\ e^{-\beta u_{\rm a}}}} \\
&= S^* \frac{\int_{\rm site} d\mathbf{r}\ \rho(\mathbf{r})\ e^{-\beta u_{\rm a}}}{\rho(r^*,0,0) \int d\mathbf{r}\ \delta(r-r^*)\ e^{-\beta u_{\rm a}}} \\
&= S^* \frac{\int_{\rm site} d\mathbf{r}\ \rho(\mathbf{r})\ e^{-\beta u_{\rm a}}}{\int d\mathbf{r}\ \delta(r-r^*)\ \rho(\mathbf{r})\ e^{-\beta u_{\rm a}}} \\
&= S^* \int_{\rm site} dr' \left[\frac{\int d\mathbf{r}\ \delta(r-r')\rho(\mathbf{r})\ e^{-\beta u_{\rm a}}}{\int d\mathbf{r}\ \delta(r-r^*)\rho(\mathbf{r})\ e^{-\beta u_{\rm a}}} \right] \\
&= S^* \int_{\rm site} dr'\ e^{-\beta[\mathcal{W}(r')-\mathcal{W}(r^*)]}. \qquad (6)
\end{aligned}$$

$\mathcal{W}(r)$ is a PMF defined as a function of the radial distance r between the ligand and the protein, computed in the presence of the applied conformational restraint on the protein, $u_{\rm p}$, and the conformational, orientational, and axial restraints on the ligand, $u_{\rm c}$, $u_{\rm o}$, and $u_{\rm a}$, respectively (see **Supplementary Fig. 1**, Online Methods, and **Supplementary Methods**),

$$e^{-\beta[\mathcal{W}(r')-\mathcal{W}(r^*)]} = \frac{\int d\mathbf{L}\ \delta(r-r') \int d\mathbf{X}\ e^{-\beta[U+u_{\rm p}+u_{\rm c}+u_{\rm o}+u_{\rm a}]}}{\int d\mathbf{L}\ \delta(r-r^*) \int d\mathbf{X}\ e^{-\beta[U+u_{\rm p}+u_{\rm c}+u_{\rm o}+u_{\rm a}]}}. \qquad (7)$$

S^* is the Jacobian, a spherical surface integral over the position of the ligand relative to the protein when it is in the bulk at a specified reference distance r^*,

$$S^* = \int d\mathbf{r}\ \delta(r - r^*)\ e^{-\beta u_{\rm a}(\theta,\phi)}$$

$$= (r^*)^2 \int_0^{\pi} \sin(\theta) d\theta \int_0^{2\pi} d\phi\ e^{-\beta u_{\rm a}(\theta,\phi)}. \quad (8)$$

In the text, $I^* \equiv \int_{\rm site} dr'\ e^{-\beta[\mathcal{W}(r')-\mathcal{W}(r^*)]}$, and C° is the standard state concentration of 1 mol/L ($\equiv$ 1/1661 Å^3). The equilibrium binding constant then becomes

$$K_{\rm eq} = S^* I^*\ e^{-\beta[\Delta G_{\rm p,bulk}+\Delta G_{\rm c,bulk}+\Delta G_{\rm o,bulk}-\Delta G_{\rm a,site}-\Delta G_{\rm o,site}-\Delta G_{\rm c,site}-\Delta G_{\rm p,site}]}. \quad (9)$$

For a receptor protein that does not undergo large conformational changes relevant to ligand binding, protein conformational restraints are unnecessary, so $u_{\rm p} = 0$. The first and last terms in **Supplementary Eq. 3** consequently vanish from the product. The resulting equation is equivalent to the $K_{\rm eq}$ of ligand binding to an inflexible protein, or ligand docking. For a flexible receptor, the change in the conformational free energy of the protein upon ligand docking is $\Delta G_{\rm p} = \Delta G_{\rm p,bulk} - \Delta G_{\rm p,site}$ (see **Supplementary Eqs. 4a,g**).

References

1. Armstrong, N. & Gouaux, E. Mechanisms for activation and antagonism of an AMPA-sensitive glutamate receptor: crystal structures of the GluR2 ligand binding core. *Neuron* **28**, 165–181 (2000).

2. Hogner, A., Kastrup, J. S., Jin, R., Liljefors, T., Mayer, M. L., Egebjerg, J., Larsen, I. K. & Gouaux, E. Structural basis for AMPA receptor activation and ligand selectivity: crystal structures of five agonist complexes with the GluR2 ligand-binding core. *J. Mol. Biol.* **322**, 93–109 (2002).

3. Holm, M. M., Lunn, M. L., Traynelis, S. F., Kastrup, J. S. & Egebjerg, J. Structural determinants of agonist-specific kinetics at the ionotropic glutamate receptor 2. *Proc. Natl. Acad. USA* **102**, 12053–12058 (2005).

4. Nielsen, B. B., Pickering, D. S., Greenwood, J. R., Brehm, L., Gajhede, M., Schousboe, A. & Kastrup, J. S. Exploring the GluR2 ligand-binding core in complex with the bicyclical AMPA analogue (S)-4-AHCP. *FEBS J.* **272**, 1639–1648 (2005).

5. Hogner, A., Greenwood, J. R., Liljefors, T., Lunn, M. L., Egebjerg, J., Larsen, I. K., Gouaux, E. & Kastrup, J. S. Competitive antagonism of AMPA receptors by ligands of different classes: crystal structure of ATPO bound to the GluR2 ligand-binding core, in comparison with DNQX. *J. Med. Chem.* **46**, 214–221 (2003).

6. Ahmed, A. H., Thompson, M. D., Fenwick, M. K., Romero, B., Loh, A. P., Jane, D. E., Sondermann, H. & Oswald, R. E. Mechanisms of antagonism of the GluR2 AMPA receptor: structure and dynamics of the complex of two willardiine antagonists with the glutamate binding domain. *Biochemistry* **48**, 3894–3903 (2009).

7. Lee, P. H., Ayyampalayam, S. N., Carreira, L. A., Shalaeva, M., Bhattachar, S., Coselmon, R., Poole, S., Gifford, E. & Lombardo, F. In silico prediction of ionization constants of drugs. *Mol. Pharm.* **4**, 498–512 (2007).

8. Liao, C. & Nicklaus, M. C. Comparison of nine programs predicting pk(a) values of pharmaceutical substances. *J. Chem. Inf. Model.* **49**, 2801–2812 (2009).

9. Bashford, D. & Karplus, M. pka's of ionizable groups in proteins: atomic detail from a continuum electrostatic model. *Biochemistry* **29**, 10219–10225 (1990).

10. Brooks, B. R. et al. CHARMM: the biomolecular simulation program. *J. Comput. Chem.* **30**, 1545–1614 (2009).

11. MacKerell, Jr., A. D. et al. All-atom empirical potential for molecular modeling and dynamics studies of proteins. *J. Phys. Chem. B* **102**, 3586–3616 (1998).

12. Jorgensen, W. L., Chandrasekhar, J., Madura, J. D., Impey, R. W. & Klein, M. L. Comparison of simple potential functions for simulating liquid water. *J. Chem. Phys.* **79**, 926–935 (1983).

13. Essmann, U., Perera, L., Berkowitz, M. L., Darden, T., Lee, H. & Pedersen, L. G. A smooth particle mesh Ewald method. *J. Chem. Phys.* **103**, 8577–8593 (1995).

14. Ryckaert, J.-P., Ciccotti, G. & Berendsen, H. J. C. Numerical integration of the cartesian equations of motion of a system with constraints: molecular dynamics of *n*-alkanes. *J. Comput. Phys.* **23**, 327–341 (1977).

15. Feller, S. E., Zhang, Y., Pastor, R. W. & Brooks, B. R. Constant pressure molecular dynamics simulation: the Langevin piston method. *J. Chem. Phys.* **103**, 4613–4621 (1995).

16. Woo, H.-J. & Roux, B. Calculation of absolute protein-ligand binding free energy from computer simulations. *Proc. Natl. Acad. Sci.* **102**, 6825–6830 (2005).